Dissertation

Establishment of a new murine CKD-MBD model and the role of autophagy in uremic vascular media calcification

submitted by

Bianca Rosa Anna Frauscher

BSc MSc

for the Academic Degree of

Doctor of Philosophy

(PhD)

at the

Medical University of Graz

Clinical Division of Nephrology

Department of Internal Medicine

under the supervision of

Assoz. Prof. Priv.Doz. Dr.med.univ. Philipp Eller, MBA

2018

Statutory Declaration

I hereby declare that this thesis is my own original work and that I have fully acknowledged by name all of those individuals and organisations that have contributed to the research for this thesis. Due acknowledgement has been made in the text to all other material used throughout this thesis and in all related publications I followed the "Standards of Good Scientific Practice at the Medical University of Graz".

Graz, September 2018

Eidesstaatliche Erklärung

Ich erkläre hiermit ehrenwörtlich, dass ich diese Arbeit selbstständig verfasst habe, und dass jene Personen und Organisationen, die an dieser Arbeit beteiligt waren, namentlich genannt sind. Benutzte Quellen wurden kenntlich gemacht, und ich habe keine anderen als die angegebenen Quellen verwendet. In der gesamten Arbeit sowie in der daraus resultierenden Publikation wurden die Regeln des „Good Scientific Practice" befolgt.

Graz, September 2018

Disclosures

Parts of this thesis have been published in peer-reviewed journals. The permission for re-print the figures has been given with the Open-Access-Publication agreements of the publishing group.

The thesis is based on the following publications:

(1) Frauscher B, Artinger K, Kirsch AH, Aringer I, Moschavaki-Filippidou F, Kétszeri M, Schabhüttl C, Rainer PP, Schmidt A, Stojakovic T, Fahrleitner-Pammer A, Rosenkranz AR, Eller P, Eller K. A New Murine Model of Chronic Kidney Disease-Mineral and Bone Disorder. International Journal of Endocrinology. 2017 (1)

(2) Frauscher B, Kirsch AH, Schabhüttl C, Schweighofer K, Kétszeri M, Pollheimer M, Dragun D, Schröder K, Rosenkranz AR, Eller K, Eller P. Autophagy Protects From Uremic Vascular Media Calcification. Frontiers in Immunology. 2018 (2).

All co-authors gave their consent to re-use data from the publications within this thesis.

This thesis project was undertaken with full financial support from the Austrian Science Fund (FWF) within the PhD program Molecular Medicine (MolMed).

Acknowledgment

Firstly, I would like to express my gratitude to my supervisor Philipp Eller as well as to Kathrin Eller for their unwavering support, guidance and insight throughout this research project.

I would like to extend my thanks to all laboratory colleagues: Katharina Artinger, Ida Aringer, Alexander Kirsch, Corinna Schabhüttl and Kerstin Schweighofer.
My special thanks and appreciation go to Máté Kétszeri, Foteini Moschovaki-Filippidou and Agnes Mooslechner for their support and friendship as well as for their positive energy and motivation over the last three years.

I owe my deepest gratitude to my family, especially my mum, for their love, patience and undying support as well as for being there for me in good and hard times during the whole PhD process.
I would like to thank my wonderful friends, especially Melanie, for her encouragement, understanding and support at various stages of my PhD studies.

My heartfelt appreciation goes to you, Matthias. You always believe in me no matter what and I am grateful for your confidence, respect and patience with everything I am doing and for your great support in thousands of matters.

Table of Contents

Abbreviations and Definitions

Adrb2	adrenergic receptor, beta 2
ATG16l1	autophagy related 16-like 1
AKI	acute kidney injury
BFR	bone formation rate
BUN	blood urea nitrogen
BV/TV	bone volume/tissue volume
CCR	C-C chemokine receptor
CD	cluster of differentiation
CD4	T cell co-receptor
CD8	T cell co-receptor
CD68	Macrophage marker
CKD	chronic kidney disease
CKD-MBD	chronic kidney disease – mineral and bone disorder
dH_2O	distilled water
DM	diabetes mellitus
ELISA	enzyme-linked immunosorbent assay
ES	ejection fraction
ES/BS	eroded surface/bone surface
ESRD	end-stage renal disease
FCS	fetal calf serum
FGF 23	fibroblast growth factor 23
FITC	fluorescein isothiocyanate
FS	fractional shorting
Foxp3	forkhead box P3, master regulator of regulatory T cells
GAPDH	glyceraldehyde 3-phosphate dehydrogenase
GATA3	GATA binding protein 3
GFR	glomerular filtration rate
HEPES	hydroxyethyl piperazineethanesulfonic acid
Hmox1	heme oxygenase 1
HPD	high phosphate diet
HPRT	hypoxanthine guanine phosphoribosyl transferase

HRP	horseradish peroxidase
Igfbp3	insulin-like growth factor binding protein 3
Il-1beta	interleukin 1 beta
Il-6	interleukin 6
KDIGO	kidney disease-improving global outcomes
(MAP1)LC3	(Microtubule-associated protein 1) light chain 3
LVEDD	left ventricular end diastolic diameter
LVESD	left ventricular end systolic diameter
MAR	mineral apposition rate
NBT	nitro blue tetrazolium
OS/BS	osteoid surface/bone surface
p62 (SQSTM1)	nucleoporin 62(Sequestome-1 protein)
PAS	periodic-Acid-Schiff
PBS	phosphate-buffered saline
PTH	parathyroid hormone
Rorc	RAR-related orphan receptor gamma
Runx2	runt related transcription factor 2, key transcription factor of osteoblast differentiation
SCD	standard chow diet
Sm22-α	smooth muscle protein 22-alpha
Tb.Sp	trabecular Separation
Tb.Th	trabecular thickness
Tb.N	trabecular number
Tbx21	T-box 21, master regulator of TH1 differentiation in mice
TH1	T helper type 1
TH2	T helper type 2
TNF	tumour-necrosis factor
Trp53	transformation related protein 53
VSMC	vascular smooth muscle cell

List of Figures

List of Tables

Abstract in German – Part A

Einleitung: Chronische Niereninsuffizienz (CKD) wird durch eine signifikante Morbidität und Mortalität charakterisiert. Eine der häufigsten Komplikationen der CKD ist ein gestörter Mineral- und Knochenstoffwechsel. Diese Störungen werden allgemein als chronic kidney disease-mineral and bone disorder (CKD-MBD) zusammengefasst. CKD-MBD ist der Hauptgrund für die extensiv ansteigende kardiovaskuläre Mortalität bei Patienten mit CKD. Wir haben ein neues nicht invasives Mausmodell für die CKD-MBD entwickelt.

Methoden: Dilute brown non-Agouti (DBA/2) Mäuse sind anfällig für ektope Nierenverkalkung, wenn sie einer erhöhten oralen Phosphatgabe ausgesetzt sind. Um einen Nierenschaden zu erzeugen, wurden diese Mäuse mit Standardfutter (SCD) oder Hochphosphatfutter für vier Tage (HPD4) oder 7 Tage (HPD7) mit sofortiger Rückkehr zu Standardfutter für 84 Tage gefüttert. Es wurden Serum und Urinproben sowie Proben von Nieren und Knochen für histologische Untersuchungen und RT-PCR gesammelt. Weiters wurden kardiovaskuläre Untersuchungen durchgeführt.

Ergebnisse: Sowohl die Mäuse der HPD4 Gruppe als auch die Mäuse der HPD7 Gruppe haben eine Phosphatnephropathie mit tubulärer Atrophie sowie interstitielle Fibrose entwickelt. Außerdem wiesen die Mäuse beider Gruppen eine signifikant reduzierte glomeruläre Filtrationsrate (GFR) sowie erhöhte Serum-Harnstoffwerte auf. Die Echokardiografie zeigte eine leichte Erhöhung der linksventrikulären Muskelmasse mit intakter linksventrikulärer systolischer Funktion. Die abdominale Aorta von HPD-Mäusen wiesen Zeichen einer Mediaverkalkung auf. Histomorphometrische Untersuchungen von HPD-Mäusen offenbarten im Gegensatz zu den SCD-Mäusen ein reduziertes Knochenvolumen/Gewebevolumen (BV/TV) sowie eine niedrigere Mineralappositions- und Knochenformationsrate. Außerdem waren die Pth- Werte in den HPD-Mäusen erhöht. Generell ist anzumerken, dass der beobachtete Phänotyp in der HPD7 Gruppe ausgeprägter war als in der HPD4 Gruppe.

Schlussfolgerung: Wir präsentieren hier ein neues, nicht invasives Modell der CKD-MBD, welches viele Merkmale des humanen Äquivalents widerspiegelt. Unser Modell ist durch Mediaverkalkung, sekundären Hyperparathyreoidismus und einer Knochenanomalie mit niedrigem Knochen-Turnover gekennzeichnet. So ist dieses Modell ein nützliches Werkzeug für die weiteren Untersuchungen von pathogenen Faktoren in der CKD-MBD ohne die Notwendigkeit von chirurgischen Methoden.

Abstract in English – Part A

Introduction: Chronic kidney disease (CKD) is characterized by long-term morbidity and mortality. We developed a murine model of CKD and evaluated the kidney-phenotype along with the systemic changes in endocrine and metabolic parameters.

Methods: DBA/2NCrl mice are susceptible to ectopic renal calcification when exposed to increased oral phosphate loads. In order to cause renal damage, these mice were fed standard chow diet or high phosphate diet for four days (HPD4) or 7 days (HPD 7) with subsequent return to SCD for 84 days Serum and urine samples, as well as samples for histology and qPCR were taken from kidney and bone. Additionally, transthoracic echocardiography was performed.

Results: CKD mice developed uremic kidney disease with marked calcification of the kidneys and a marked reduction in measured glomerular filtration rate (GFR) as determined by FITC-inulin clearance. Echocardiographic evaluations revealed a trend of an increase of left ventricle mass, whereas left-ventricular function was not affected. The abdominal aorta in HPD fed mice showed signs of media calcification. Histomorphometrical analysis revealed reduced bone volume/tissue volume (BV/TV) as well as a decreased mineral apposition rate (MAR) in HPD mice when compared with SCD mice. Additionally, serum Pth levels were increased in HPD mice. The described phenotype was more pronounced in mice from the HPD7 group than in mice from HPD4 group.

Conclusion: We here present a model of chronic kidney disease-mineral and bone disorder which reflects important features of the human equivalent. Our model is characterized by media calcification, secondary hyperparathyroidism and low-turnover bone disease. This animal model may serve as useful tool for the investigation of pathogenic features of CKD-MBD without the need for surgical methods.

Abstract in German – Part B

Einleitung: Chronische Niereninsuffizienz und Diabetes mellitus sind mit einer starken Verkalkung der *Tunica media* verbunden. Die Verkalkung der *Tunica media* wird nicht nur von systemischen Faktoren wie Hyperphosphatämie oder Hyperglykämie bestimmt, sondern ist auch von den vaskulären glatten Muskelzellen abhängig. Das Ziel unserer Untersuchungen war es die Rolle der Autophagie in der Pathogenese der urämischen Mediaverkalkung zu untersuchen.

Methoden: DBA/2NCrl Mäuse werden für 5 oder 12 Tage mit Hochphosphatfutter behandelt. DBA/2 Mäuse welche Standardfutter bekommen, dienen als Kontrolle. Um die Autophagie zu beeinflussen, wurde den Mäusen am Tag -3 Rapamycin (0.5 mg/kg Körpergewicht) intraperitoneal injiziert. Für *in vitro* Untersuchungen wurden vaskuläre glatte Muskelzellen (MOVAS) verwendet. Das Medium wurde mit Ascorbinsäure und β-Glycerolphosphat versehen, um eine Verkalkung hervorzurufen. Um die Autophagie zu beeinflussen wurden die Zellen mit entweder Rapamycin, 3-Methyladenin oder Bafilomycin behandelt. Sowohl die Aorten der DBA/2 Mäuse als auch MOVAS wurden mit Hilfe von qPCR, Western Blot, histologischen Techniken untersucht.

Ergebnisse: DBA/2NCrl Mäuse welche HPD bekamen, entwickelten eine schwere vaskuläre Verkalkung und auch die Zellen unter Verkalkungsbedingungen wiesen starke Verkalkungen auf. qPCR Analysen von Mausaorten, welche HPD bekamen, zeigten eine signifikant erhöhte Geneexpression von Autopahgie bezogenen Genen auf. Proteinwerte von LC3-II waren in den Aorten der HPD Mäuse signifikant erhöht und die dazugehörenden p62 Werte erniedrigt. Histologische Untersuchungen, zeigten dass die Autophagie vor allem in der *Tunica media* der Aorten lokalisiert war und diese mit der Dauer der Verabreichung der HPD anstieg. Die Behandlung mit Rapamycin erhöhte die Autophagie sowohl im Maus- als auch im Zellmodell. Die Behandlung mit Rapamycin hatte eine signifikante Reduzierung der Verkalkung *in vitro* und *in vivo* zur Folge. Außerdem hatten HPD Mäuse, welche mit Rapamycin behandelt wurden, eine höhere Überlebensrate als HPD Mäuse, welche mit Vehicle behandelt wurden.

Schlussfolgerung: Diese Ergebnisse beweisen, dass die Autophagie eine wichtige Rolle bei der Entstehung der urämischen Mediaverkalkung einnimmt. Außerdem schützt die Autophagie, wenn sie durch Rapamycin erhöht wird, vaskuläre glatte Muskelzellen als auch Mausaorten vor der Verkalkung.

Abstract in English – Part B

Introduction: Chronic kidney disease and diabetes mellitus are associated with extensive media calcification. The calcification of the tunica media is not only driven by systemic factors such as hyperphosphatemia and hyperglycemia, but is also dependent on vascular smooth muscle cells. The aim of our study was to investigate the role of autophagy in the pathogenesis of uremic media calcification.

Methods: DBA/2NCrl mice were fed with high phosphate diet (HPD) for 5 or 12 days. DBA2/N mice on standard chow diet (SCD) were used as controls. To influence autophagy mice were treated intraperitoneally with 0.5 mg rapamycin per kg body weight starting on day -3. For our in vitro experiments, mouse muscular smooth muscle cells (MOVAS) were used. The medium was supplemented with ascorbin acid and β-glycerolphosphate to induce calcification. To influence autophagy, cells were treated with rapamycin or 3-methyladenin or bafilomycin. Aorta samples as well as MOVAS were analyzed using qPCR, Western Blot, and histology.

Results: DBA2/NCrl mice on HPD developed a severe vascular calcification and also the cells showed calcification in presence of calcifying medium. qPCR of mouse aortas revealed a significantly higher gene expression of autophagy related genes such as *igfbp3* or *trp53in* on day 5 and 12 on HPD. The protein levels of the autophagy markers LC3-II/I were also significantly increased in aortas of mice on HPD. In line protein levels of p62 were downregulated. By using histological staining, we showed that autophagy is located in the tunica media of the aortas and that it increases with the time on HPD. Rapamycin treatment further increased autophagy in vivo and in vitro. Rapamycin treatment resulted in a significant decrease of vascular calcification *in vivo* and *in vitro*. Furthermore, Rapamycin-treated mice survived longer compared to vehicle-treated controls.

Conclusion: These findings indicate that autophagy plays an important role in the development of uremic media calcification. Furthermore, induction of autophagy by Rapamycin protects cells and mice from uremic media calcification.

General Introduction

Chronic kidney disease

Prevalence of kidney disease

The 2012 Kidney Disease – Improving Global Outcome (KDIGO) clinical practice guideline for the evaluation and management of chronic kidney disease (CKD) define kidney disease "as an abnormality of kidney structure or function with implications for the health of an individual, which can occur abruptly, and either resolve or become chronic"(3).

Acute kidney injury (AKI) is described as an abrupt, within hours, decrease in kidney function, which includes both structural damage and loss of kidney function. AKI might resolve or might lead to various complications, such as metabolic acidosis or uremia, resulting in death (4). CKD is a worldwide health burden with increasing economic cost to health system and with a risk factor for end stage renal disease (ESRD) resulting in the need of renal replacement therapy (5).

A meta-analysis of 100 studies since 2001, covering 112 populations, displayed that a globally CKD prevalence stage 1 to 5 was 13.4% and 10.6% in stages 3 to 5. These findings indicate that CKD is more common than diabetes, which has an estimated prevalence of 8,2% (5). Of note, women were more affected by CKD than men (5).
Nevertheless, for CKD management per se, the geographic region, age and race as well as ethnicity should be considered. An extensive difference in both CKD stages 1-5 and CKD stages 3-5 prevalence in Europe was found. The adjusted CKD stages 1-5 prevalence ranged from 3.31% in Norway to 17.3% in northeast Germany. The adjusted CKD stages 3-5 prevalence varied between 1.0% in central Italy and 5.9% in northeast Germany (6).
The incidence rate of AKI is poorly known because of missing documentation, regional disparities and differences in definition (7). Still, epidemiological studies reported 1811 incidences of AKI per million population (8).

Definition and classification of CKD

The conceptual model of CKD was developed by the National Kidney Foundation's Kidney Disease Quality Outcome Initiative in 2002 and was revised and adopted by the international consensus of KDIGO in 2005. This worldwide accepted model includes initial kidney damage, which is followed by a reduction of glomerular filtration rate (GFR) and finally leads to kidney failure (9). The development and progression of CKD evolves over a long time and is marked by a latency period without symptoms, before decreased kidney function causes late onset of symptoms (9).

This conceptual model as well as the KDIGO guidelines are responsible for defining the criteria of CKD. Thus, CKD is defined as kidney damage or GFR <60 mL/min/1.73 m^2 for a period of 3 months or more (10). Kidney damage per se is defined as structural or functional abnormality of the kidney (10). Structural or functional abnormalities are described by pathological abnormalities and altered markers of kidney damage. This markers include history of kidney transplantation, urine abnormalities, such as albuminuria, blood abnormalities such as renal tubular syndromes, or imaging abnormalities like polycystic kidney or hydronephrosis (9). Albuminuria is one of the most important criteria, for defining CKD. It is an early marker of kidney damage due to diabetes, glomerular disease as well as hypertension and reflects increased glomerular permeability. On the one hand high levels are associated with adverse outcomes, including progression of kidney and cardiovascular disease. On the other hand therapies that reduces albuminuria are associated with a slower the progression of kidney disease (9).

Besides of albuminuria, GFR seems to be the best overall index to characterize kidney function in health and disease. The only disadvantage is that GFR measurement is difficult to perform. This why in the clinical practice, GFR is estimated from serum creatinine concentrations (9). Generally low GFR levels are scarce in the young population under 40 years, but low levels are linked with increasing complications of CKD as well as adverse outcomes, including cardiovascular diseases, morbidity and mortality (9).
Furthermore, a combination of GFR levels and albuminuria categories is used to define the stage of CKD in order to permit the best treatment strategies for patients suffering from CKD.

Therefore, the KDIGO 2012 guidelines estimate the prognosis of CKD depending on GFR categories and categories of albuminuria (3, 11). GFR categories are divided into G1 (≥90 ml/min/1.73 m^2, normal or high), G2 (60-89 ml/min/1.73 m^2, mildly decreased), G3a (45-59 ml/min/1.73 m^2, mildly to moderately decreased), G3b (30-44 ml/min/1.73 m^2, moderately to severely decreased), G4 (15-29 ml/min/1.73 m^2, severely decreased) and G5 (<15 ml/min/1.73 m^2, kidney failure) (3, 11).
The categories of albuminuria are A1 (<30 mg/g creatinine, normal to mildly increased), A2 (20-300 mg/g creatinine, moderately increased) and A3 (>300 mg/g creatinine, severely increased) (3, 11).

For example, on the one hand GFR categories G1 and G2 in combination with an albuminuria category A1 are marked with a low risk, but on the other hand the same GFR categories linked with an albuminuria category A2 are characterized by a moderately increased risk. However, patients with a GFR of category G1 or G2 and with an albuminuria of category A3 are diagnosed with a high risk (3, 11).

The separation of CKD stage 3 into CKD G3a and G3b is essential, because in stage 3 an increase of the mortality rate is observed (12). Especially the risk of cardiovascular events resulting in an increased risk of death increases massively between CKD G3a and G3b (13).
A lot of symptoms occur only in progressed CKD, especially in patients with CKD stages 4 to 5. Side effects of decreased GFR include hypertension, anemia, malnutrition, bone and mineral disorder as well as general decreased quality of life (9). The burden of these complications highlights the importance to start with therapeutic interventions at early stages of CKD in order to prevent or improve complications of decreased GFR.

Risk factors for development of CKD

Since CKD is a worldwide health issue, the identification and understanding of risk factors for the development of CKD are very important (14).
Nowadays, in both developed and developing countries, diabetes mellitus (DM) is the leading cause of CKD as well as ESRD. The underlying mechanisms that lead to the loss of kidney function in DM includes hyperfiltration injury and various molecular changes, which are linked to diabetic nephropathy (14, 15). Already 8% of new patients suffering from type 2 diabetes additionally have proteinuria (14, 15). When patients with type 2 DM develop proteinuria, their 10-year risk of developing progressive CKD is 11% (14, 16). Thus, albuminuria plays an important role in DM, since it is also a main predictor for mortality in type 2 DM (17). Furthermore 50% patients with type 2 DM will develop diabetic nephropathy and 10% of these patients will progressively loose their kidney function (14).

Another strong risk factor for development of CKD as well as for ESRD is hypertension, since the risk for developing ESRD increases proportionally with increasing severity of high blood pressure (18). Of note, hypertension can be either a cause or a consequence of CKD (19) . Still, high blood pressure is a driving force in decreasing GFR in diabetic as well as in nondiabetic kidney disease and it is also an independent risk factor for the development of ESRD (19) .One mechanism of hypertension-related renal damage includes the systemic high blood pressure, which its transmitted to the kidney vasculature and eventually leads to a local barotrauma (19). Another mechanism is that the systemic high blood pressure is transmitted to the kidney and results in mechanical stretch of glomerular capillaries and mesangial cells, which induces a repair mechanism leading to glomerulosclerosis (19).

Obesity has been revealed to be one of the strongest modifiable risk factors for ESRD in the last years (20). The increased metabolic needs in patients, may leads to increased capillary glomerular pressure with following development of glomerulosclerosis (20). An epidemiologic study from Sweden demonstrated that obesity (BMI $\geq$ 30 kg/m^2) in men and morbid obesity (BMI $\geq$ 35 kg/m^2) among women lead to three- to fourfold higher risk to develop CKD (21) .

Low birth weight has been shown to be related to the development of CKD as well. Thus, a low birth weight is linked to low nephron numbers, which may result in intraglomerular hypertension and hyperfiltration in the remaining nephrons leading to low GFR levels (22, 23).

Experiencing acute kidney injury as well as a family history or genetic factors such as those causing polycystic kidney disease are additional risk factor for the development of CKD (14). Furthermore, gender, age and ethnicity play a role in the odds to develop CKD. Thus, it is known that the risk for the development of ESRD in African Americans is higher when compared with Caucasians and that renal function declines with age (14).

The understanding of all these different risk factors for CKD and ESRD will increase early detection an may help to find the appropriate treatment for CKD (14).

Chronic kidney disease-mineral and bone disorder

One of the most frequent complications of CKD is a disturbance of the mineral and bone metabolism, which are collectively referred to as chronic kidney disease-mineral and bone disorder (CKD-MBD) (24). These changes include biochemical abnormalities in calcium, phosphate, parathyroid hormone (PTH), fibroblast growth factor 23 (FGF-23) and vitamin D, bone abnormalities, such as changes in morphology, volume or mineralization, and vascular calcification as well as soft tissue calcification (24, 25).

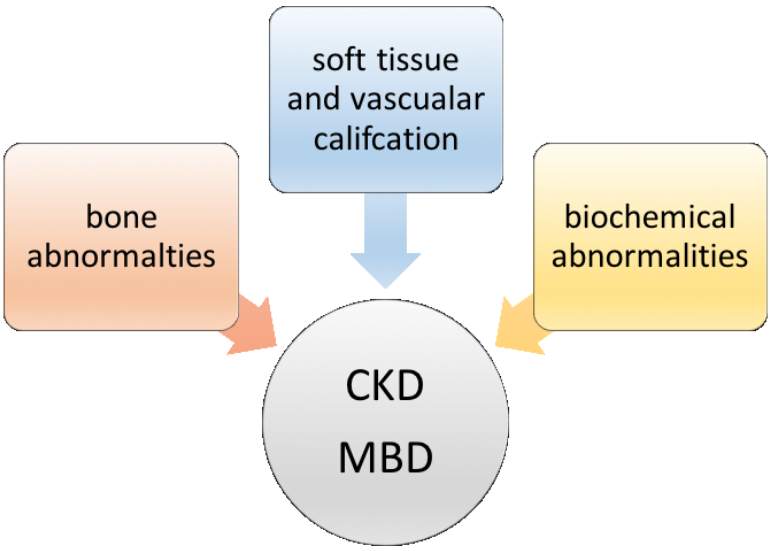

Figure 1: Chronic kidney disease-mineral and bone disorder.

Biochemical abnormalities, bone abnormalities as well as soft and vascular calcification occur in CKD-MBD. Adopted from *Nigwekar et al. (25)*

Biochemical abnormalities: balance of calcium and phosphate metabolism

The mineral and bone metabolism is regulated by calcium, phosphate, PTH, FGF-23 and vitamin D related compounds (26). Alteration of these key players of the mineral homeostasis often result in hypocalcaemia, hyperphosphatemia, hyperparathyroidism, increased FGF-23 or hypovitaminosis D (27).

Phosphorus is an essential element that is necessary for many biological processes (28). Thus, compounds containing phosphorus are involved in cell structure, cellular metabolism, balancing of acid-base homeostasis as well as bone mineralization (29). In the human body phosphate is the most abundant anion and accounts for approximately 1% of total body weight. It mostly occurs intracellular with a concentration which is 100-fold greater than that of the plasma (29, 30). Around 85% of the total phosphate is bound in bone and teeth, 14% of phosphate is distributed between tissue, while 1% is in the extracellular fluid (29, 30). The control of serum phosphate is essential to avoid metabolic disorders (31). Since phosphate occurs as free anionic phosphate, it can be filtered across the glomerular size- and charge-specific barrier. Thus, the kidney is the key regulator to balance the phosphorus homeostasis, as changes in tubular reabsorption result in precise regulation of phosphate balance in the whole human body (31). The glomerular filtration is followed by reabsorption of phosphorus in the proximal tubule. The needed sodium phosphate antiporters are controlled by PTH, 1,25-OH vitamin D and FGF-23. In healthy individuals the precise phosphate handling leads to an accurate regulation of bone metabolism (31). In patients with a loss of kidney function, an increase of free phosphate is observed, since the kidney is not able to excrete the appropriate amount of phosphate. Upon increases in the levels of free phosphate osteocytes are stimulated to release FGF-23. FGF-23 increases the fractional excretion of phosphate and inhibits the hydroxylation from 25-(OH)-vitamin D to active 1,25-$(OH)_2$-viatmin D (31). Therefore, FGF-23 counteracts the activity of vitamin D and PTH. Due to decreased calcium levels, the synthesis of PTH is stimulated. The reduction of calcium levels is detected by the calcium sensing receptor on the parathyroid gland, whereupon increasing amounts of PTH are released (29-31). This process results in a release of calcium from the bone, since PTH activates osteoblasts, which leads to an activation of osteoclasts. Additionally, PTH increases the intestinal and tubular calcium and phosphate reabsorption, as it raises the availability of active Vitamin D by boosting the activity of 1a-hydroxylase. This enzyme catalyzes the hydroxylation from 25-OH vitamin D to active 1,25-$(OH)_2$-viatmin D (31).

One of the earliest signs of a disturbed in mineral and bone metabolism is an increase of serum FGF-23 levels (32, 33). A cross-sectional study demonstrated, that increased FGF-23 is a common manifestation in patients with early CKD because of that, patients are able to increase fractional phosphate excretion to prevent phosphate retention (32).

Other characteristics of a disturbance in mineral and bone metabolism are alterations in vitamin D and PTH metabolism (32, 33), elevated phosphate levels (34) and decreased levels of FGF-23 coreceptor Klotho (35).

Bone abnormalities

Already in its early stages, CKD is accompanied by a disturbed mineral and bone metabolism. Therefore, patients with CKD as well as ESRD have an increased risk for bone loss resulting in various forms of renal bone disease (36). Furthermore, fractures are common in patients suffering from CKD and associated with high morbidity and mortality (37). The United States Renal Data System reported a four-fold increased risk for hip fractures in patients on hemodialysis (38).

Renal osteodystrophy is the term that has been used in the past to describe the abnormalities in bone morphology that developed in CKD. Nowadays this traditional definition of renal osteodystrophy no longer completely describes the underlying bone pathology and does not cover all symptoms which are related to CKD-MBD (24). Therefore, the KDIGO guideline defines renal osteodystrophy as one measure of the skeletal component of the mineral and bone disorder that occur as a complication of CKD (10, 24). Renal osteodystrophy describes the alteration of bone morphology in patients with CKD and is evaluated by histomorphometry and bone biopsy (24).

The bone abnormalities display a wide spectrum of different forms. In order to describe the various types of renal osteodystrophy three histological descriptors are used: bone turnover, mineralization and volume (24). This TMV classification system helps do define the pathophysiology and to find appropriate therapy strategy (10, 24).

Turnover	Mineralization	Volume
low		low
	normal	
normal		normal
	abnormal	
high		high

Table 1: TMV classification system.

TMV classification system: Turnover, mineralization and volume are used to describe the bone phenotype in renal osteodystrophy. Adopted from *Moe et al.* (24)

A healthy bone is a dynamic tissue which resorbs old bone tissue and replaces it with new bone. Thus, the turnover is determined the rate of bone formation, which is in a healthy bone that is in balance is the same as the rate of bone resorption (39). In patients without any bone disease, the osteoblasts lay down new collagen, followed by mineralization of the matrix. In patients with CKD this process can be delayed or disorganized. Thus the mineralization describes the extent to which surface is mineralized (39, 40). The bone density reflects the volumetric proportion of osteoids and is referred as bone volume. (40)

Nevertheless, finding the appropriate diagnosis is still difficult since the spectrum of bone disease in patients with CKD and ESRD is widely spread. CKD patients may suffer from a bone disorder marked by high bone-turnover with a normal mineralization (41). This type, namely osteitis, is often depends on a secondary hyperparathyroidism (24, 41). Other alterations are characterized by low bone-turnover and decreased mineralization rates such as osteomalcia, which is often accompanied by a deficiency of vitamin D (41, 42). Furthermore, adynamic bone disorder may occur which is marked by a low turnover associated with normal mineralization and decreased bone volume (43).

Vascular calcification as risk factor

CKD and ESRD increase the risk of cardiovascular diseases as well as the risk of death (13). Thus, the cardiovascular mortality risk of patients suffering from ESRD is 5 to 10-fold higher than in the general population (44, 45). Vascular calcification is highly prevalent in patients with ESRD, occurs many years earlier than in the general population and causes this high mortality and morbidity rate (44). Vascular calcification per se is an abnormal disposition of calcium in valves, blood vessel and the heart (46, 47). One of the challenges is that the progression of vascular calcification rapidly accelerates once patients start with dialysis (48).

Calcification affects both the intimal and medial layers of vasculature, although media calcification is more common in patients with CKD and ESRD (46). Calcification of the *tunica intima* reflects atherosclerosis and is accompanied by inflammatory processes (49, 50). The prototype of media calcification is called Monckeberg's sclerosis and is related to aging, diabetes mellitus as well as to CKD (46). Calcification of the *tunica media* displays a diffuse mineral deposition throughout the vascular tree and is characterized by reduced

arterial distensibility (44). This arterial stiffness causes high blood pressure and leads to a reduction of coronary perfusion resulting in a left ventricular hypertrophy followed by an increased risk of heart failure and cardiovascular mortality (44).

Development of media calcification can be independent of both atherosclerosis and increased levels of calcium and phosphate, since it can also result from a change in the phenotype of vascular smooth muscle cells (VSMCs) (44, 51).
VSMCs origin from the mesenchyme and are therefore able to differentiate into other mesenchymal-derived cells upon stress or injury (52). Vascular calcification is based on the differentiation of contractile VSMCs into a chondrocyte or osteoblastic phenotype. This process is driven by active inducers, such as bone morphogenic protein 2 (BMP-2), an inducer of differentiation of VSMCs to osteoblast-like cells or run-related transcription factor 2 (Runx2), a transcription factor for osteoblast differentiation (44, 53). Due to a shifted balance in CKD and ESRD these active inducers are upregulated. In a non-disturbed mineral and bone metabolism, these active inducers are counteracted by various inhibitors of vascular calcification, such as fetuin-A or matrix gla protein (44). Finally, this shift in the balance of inhibitors and promotors results in development of media calcification.

Autophagy

Autophagy is an evolutionary conserved mechanism that involves cellular degradation and recycling and occurs in all eukaryotes. Autophagy plays an important role in cell survival and maintenance due to be a key regulator of degradation of cytoplasmic organelles, proteins and of recycling of breakdown products (54). In mammalian cells three main types of autophagy exist: microautophagy, macroautophagy and chaperone-mediated autophagy(55).

Microautophagy

Microautophagy is defined as lysosomal vacuolar membrane dynamics to transport cytosolic components into the lumen of lytic organelle (56). The cytoplasmic contents enter the lysosome through an invagination or deformation of the lysosomal membrane (54). Previous data reported that a process called endosomal microautophagy is able to transport soluble cystolic proteins to the vesicles of late endosomal multivesicular bodies (57).

Chaperon-mediated autophagy

Chaperon-mediated autophagy (CMA) is a proteolytic system which contributes to degradation of intracellular proteins in lysosomes (54, 58). The substrate proteins of CMA are specific to lysosomes and because of the coordinated process of chaperones located at both sides of the membrane they are able to translocate into the lysosomal lumen (58). The selectivity of CMA leads to a degradation of specific proteins resulting in supporting specific enzymatic metabolic processes. Furthermore, CMA plays a role in the cellular quality control, since CMA is responsible for removing damaged or malfunctioning proteins (58).

Macroautophagy

Macroautophagy is the most extensively explored autophagy process. The initial step of macroautophagy is the formation of an isolation membrane, called phagophore, which originates from different intracellular membrane sources. The formation of the isolation membrane is followed by elongation and finally leads to a complete autophagosome. The next step is the fusion of lysosomes with autophagosomes and results in the formation of autolysosomes. In these autolysosomes the autophagic substrates are exposed to the hydrolytic interior of lysosomes which leads to their own degradation (59) (60).
Dysfunction of macroautophagy is associated with both physiological and pathological conditions. Nowadays, around 38 autophgay-related genes are identified which control the complex process of autophagy in yeast. Approximately 50% of these genes are conserved up to human and there are additional genes with a function in higher eukaryotes that are not found in yeast. Furthermore, this regulatory process provides new therapeutic strategies for many diseases (61).

LC3 and p62

MAP1LC3/LC1 (microtubule-associated protein 1 light chain 3) is the mammalian equivalent to yeast Atg8 and is often used as marker to explore the role of autophagy (62). It is a key regulator of the whole autophagy process, since LC3 initiates autophagosome biogenesis. Still, the role of LC3 in autophagy is heavily discussed. Under nutrient-rich conditions, LC3 occurs in an acetylated form in both the nucleus and cytoplasm. Starving conditions lead to the redistribution of LC3 from the nucleus to the cytoplasm. This relocation is associated with the deacetylation of the protein by the activated nuclear deacetylase SITRT1 and with its nuclear interaction partner TP53INP2/DOR. This deacetylation is necessary for LC3 to bind to ATG7 for the subsequent lipidation. This indicates that the nuclear accumulation of LC3 is the primary source of membrane-conjugated LC3 and that starving conditions may result in an induction of autophagy (63).

p62/SQSTM1 is a multifunctional protein and is involved in many cellular processes such as signal transduction or degradation of proteins and organelles (64, 65). p62 acts as a scaffold to bring together various components during a signaling pathway and plays an important role in the autophagic process (66). p62 directly binds to LC3 and is itself degraded by autophagy. Ubiquitinated proteins are degraded in the lysosome during the autophagic process since p62 is able to link these proteins to the autophagic machinery (67).

Part A - A new Murine Model of Chronic Kidney Disease-Mineral and Bone Disorder

Introduction

Chronic kidney disease (CKD) is a global health burden with an increasing incidence and prevalence (68). The US Renal Data System 2017 Annual Data Report revealed that 14.8% of the US adult population has chronic kidney disease (69).

Chronic kidney disease, especially end-stage renal disease (ESRD) is characterized by high cardiovascular morbidity and overall mortality. (13) The leading cause of mortality of patients with CKD as well as ESRD are cardiovascular diseases. This immense risk of cardiovascular disease is related to reduced vascular compliance, left ventricular hypertrophy, extensive arterial calcification and sudden cardiac death (70, 71). Non-uremic subjects develop arterial calcification, which characteristically affects intimal atherosclerotic plaques. In contrast CKD patients primarily develop a calcification of the *tunica media*, which is mainly present in the smooth muscle layers of large and medium-sized arteries (72-74). Hence, uremic vascular media calcification and atherosclerotic intima calcification are distinct entities in CKD (73).

The major driving force for the occurrence of media calcification is a disturbed mineral and bone metabolism (24, 75). Failing kidney function means that there is a dynamic deregulation in mineral homeostasis. This deterioration in mineral metabolism leads to a disturbance of the concentration of phosphorus and calcium levels in serum as well as in tissue and to alterations in circulating levels of hormones (75). These involve changes in values of parathyroid hormone (PTH), fibroblast-growth factor-23 (FGF-23), 25-hydroxyvitamin D (25(OH)D) as well as 1,25-dihydroxyvitamin D ($1,25(OH)_2D$) (75).

This loss of mineral and endocrine function in patients with CKD affects the initial bone formation during growth and also the bone structure and function during adulthood. These disturbed processes of bone modeling as well as bone remodeling lead to the occurrence of

bone abnormalities, which occurs in nearly all patients requiring dialysis and in most of the patients with CKD stage 3-5 (24, 75).
This triad of altered biochemical parameters, vascular calcification and bone abnormalities associated with CKD is collectively referred as chronic kidney disease-mineral and bone disorder (CKD-MBD) (43, 75).

Thus, the majority of patients with CKD develop renal bone disease. The spectrum of renal osteodystrophy is wide and has changed over the past 20 years (43). Renal bone disease varies from low-turnover adynamic bone disease to high-turnover osteitis fibrosa (24, 43). Over the last twenty years a dominance of high-turnover bone disease in patients with CKD stage D5 has been observed (43, 76-78). In contrast, nowadays 40-70% of CKD patients develop a low-turnover bone disease (43, 79, 80). One explanation for this change is a higher expectancy of life in patients treated with dialysis and an increased prevalence of diabetes mellitus in CKD patients (43). Of note, also more than one type of renal bone disease can coexist in the same patient with CKD (24).

Determining the appropriate treatment in CKD patients with bone disease can be challenging. Untreated patients with increasing bone turnover develop hyperparathyroid bone disease. In contrast treatment with calcium or vitamin D receptor activators (VDRAs) can result in low turn-over adynamic bone disease (43). Particularly, patients with adynamic bone disorder are susceptible to develop vascular calcification (81, 82).
Finally, all forms of renal osteodystrophy are associated with bone loss and lead to a weakened bone with an increasing risk of bone fractures, especially hip fractures in patients with CKD (38, 43, 83).

Another challenge during the treatment of CKD patients is that biochemical analysis for determination of biomarkers such as PTH, FGF-23 and alkaline phosphate are not appropriate to predict renal bone disorders. On the contrary, evaluation of bone turnover, bone mineralization and bone volume based on bone biopsy followed by bone histomorphometry is the most precise method to diagnose renal osteodystrophy. However, the KDIGO guidelines advise to not routinely and improvidently perform bone biopsies in patients suffering from ESRD (24, 75).

There have, however, been few randomized controlled trials have exploring various treatment methods depending on different types of bone disorder. Thus, *in vivo* models of CKD-MBD are definitely essential to investigate and evaluate the potential of therapeutic approaches in vascular calcification as well as renal bone disorder (1). Previously, a murine CKD model with subtotal nephrectomy has been published. *Cejak et al*. showed that mice with induced CKD develop uremic osteodystrophy as well as abnormalities in bone volume accompanied by delayed mineralization (84).

For our CKD-MBD model, we used DBA/2 mice, who are susceptible to develop renal calcification when exposed to increased oral phosphate loads (85). DBA/2 mice have an alternative splice variant of the *Abcc6* gene, which encodes the *ABCC6* protein, a member of the ATP binding (ABC) cassette family of proteins and an orphan transmembrane transporter. The *Abcc6* gene is expressed primarily in the basolateral surface of hepatocytes and basal membranes of renal proximal tubules (86-90).
In the present study, we describe a new, noninvasive murine CKD-MBD model, which is characterized by secondary hyperparathyroidism and uremic media calcification. In contrast to the CKD model from *Cejak et al.*, our model displayed a low-turnover bone disease in DBA/2 mice (1).

Material and Methods

Study design

Female eight-week-old dilute-brown agouti 2 (DBA/2NCrl, hereafter referred to as DBA/2) mice were obtained from Charles River (Sulzfeld, Germany). They were housed in a virus- and antibody-free environment at the Medical University of Graz. DBA/2 mice are susceptible to ectopic renal calcification and media calcification when exposed to increased oral phosphate, due to the fact that DBA/2 mice have an alternative splice variant of the *Abcc6* gene (2, 85, 88, 89). We decided to study female DBA/2 mice because they are more prone to develop calcification than their male littermates (91, 92). To induce renal damage, the mice were fed high-phosphate diet for 4 (HPD4) or 7 (HPD7) days with subsequent return to standard chow for 84 days. The control group (SCD) was set on standard chow diet for the whole experiment. (1) The high-phosphate diet (Altromin, Lage, Germany) contained 20.2 g of phosphorus, 9.4 g of calcium, 0.7 g of magnesium, and 500 IU/kg of vitamin D3. The standard chow contained 7.0 g of phosphorus, 10.0 g of calcium, 2.2 g of magnesium and 1000 IU/kg of vitamin D3.

All animal experiments were approved by the Committee of the Ethics of Animal Experiments of the Austrian Ministry (BMWFW-66.010/0061-WF/V/3b/2016). All experiments were conducted under strict adherence to Austrian law. (1)

Biochemical evaluations

Metabolic studies included measurements of serum urea, serum fibroblast growth factor 23 (Fgf-23) and serum parathyroid hormone (Pth). (1) At the end of the experiment blood was obtained from anaesthetized mice by retro-orbital bleeding. Serum urea levels were determined with standard laboratory techniques and Fgf-23 levels (Immutopics International, San Clemente, CA, USA) as well as Pth levels (Immutopics International) were measured using commercially available enzyme-linked immunosorbent assay kits. Briefly, a sufficient number of streptavidin coated strips were placed in a holder and 20 µL of standard, control as well as sample were pipetted into wells. Next 50 µL of the working

antibody solution (1:1 mouse biotinylated antibody and mouse HRP (horseradish peroxidase) conjugated antibody) were pipetted into each well. The plates were covered with a plate sealer, then covered with aluminium foil to avoid exposure to light and incubated for three hours on a horizontal rotator at room temperature. After five times washing using the wash-solution, 100 µL of ELISA HRP substrate was pipetted into each well and incubated for 30 minutes at room temperature in the dark. Thereafter plates were read at OD 450 nm with wavelength correction (subtraction of absorbance at 620 nm) against the 0 pg/mL standard as a blank. To determine high sample concentrations, 50 µL of ELISA stop solution was pipetted into each well and the absorbance was read at 450 nm against a reagent blank of 100 µL of substrate and 50 µL of stop solution. Concentrations of Fgf-23 and Pth were determined from standard curves using log-log regression analysis. (1)

Evaluation of Histopathology

For fixation, aortas and renal tissue were stored in 4 % formalin for two days. (1) Next, samples were dehydrated and paraffin wax embedded using a Histokinette tissue processor. Kidneys and aortas were cut in 4 µm sections on a rotation microtome. Alizarin Red S and Picrosirius red staining were performed. In short, for Alizarin Red S staining rehydrated paraffin sections were incubated in 2 % Alizarin Red S solution (Sigma-Aldrich, St. Louis, MO, USA) and subsequently rinsed in acetone and acetone-xylene (1:1). For Picrosirius red staining, rehydrated renal paraffin sections were incubated in 0.1 % Picrosirius Red solution (Sigma-Aldrich).

Evaluation of Histomorphometry

For evaluation of the bone metabolism histomorphometrical analysis of murine tibia was performed (1). To measure bone formation parameters, mice were intraperitoneally injected with 20 mg/kg body weight of calcein (Sigma-Aldrich) on day 7 and day 2 before tissue harvesting. Thereafter, the bone samples were cleaned of soft tissue, fixed in 4 % formalin dehydrated in graded ethanol (70 to 100 %) and embedded in methyl methacrylate. Plastic tissue blocks were cut in 5 µm sections. For additional analysis

toluidine blue staining was performed. (1) Briefly, dewaxed and hydrated bone sections were incubated in toluidine blue working solution (1 % Toluidine Blue O (Sigma-Aldrich), 2.5 % sodium carbonate, 70 % ethanol) for five minutes. Next, sections were washed in dH_2O, dehydrated in n-Butyl acetate, mounted in anhydrous mounting medium Roti-Histokitt II (Carl Roth, Karlsruhe, Germany). Bone histomorphometric parameters were determined using OsteoMeasure^{TM} Software (OsteoMetrics, Decatur, GA, USA).

Evaluation of Immunohistochemistry

For the detection of $CD4^+$ and $CD8^+$ T cells as well as $CD68^+$ macrophages a three-layered immunoperoxidase staining technique was performed (1). Renal tissue was frozen in OCT medium and cut into 4 µm frozen tissue sections on a cryomicrotome. Slides were stored at -20°C and warmed to room temperature 30 minutes prior to staining. For fixation, slides were incubated in acetone (4°C) and subsequently blocked in 10 % serum of second antibody species, 20 % fetal calf serum, 70 % PBS and 200 µL/mL Avidin (Vector Laboratories, Burlingame, CA, USA) for 20 minutes at room temperature. After two times washing in PBS and once in gelatine, slides were incubated with respective first antibodies diluted in PBS containing 200 µL/mL Biotin (Vector Laboratories). For the detection of $CD4^+$ and $CD8^+$ T cells a rat anti-mouse CD4 mAB (Serotec, Oxford, UK) and a rat anti-mouse CD8 mAB (Serotec, UK) were used. For the detection of CD68 macrophages a rat-derived anti-mouse CD68 mAB (Serotec, UK) was used. Following one hour incubation at room temperature slides were washed three times in PBS and thereafter incubated with biotinylated goat anti-rat IgG secondary antibody (Jackson Immuno Research Laboratories, West Grove, PA, USA) for 45 minutes. After three washing steps in PBS slides were incubated in Vactastain ABC HRP kit (Vector Laboratories) for another 45 minutes. Next, slides were washed three times in PBS and once in 0.1 M sodium-acetate buffer and subsequently developed in 0.4 % 3-amino-9-ethylcarbazole for 6-8 minutes. Thereafter, slides were washed three times in PBS, counterstained in Gill's hematoxylin III (Sigma-Aldrich) and rinsed in tap water and dH_2O. Finally, slides were mounted in Aquatex mounting medium (Merck, Kenilworth, NJ, USA).

All evaluations of immunohistochemistry were performed in a blinded manner. For quantification of kidney infiltrating $CD4^+$, $CD8^+$ T cells, positive stained cells were counted in 6 high-power fields of renal and cortex and medulla. (1). Kidney infiltrating macrophages were evaluated using a semiquantitative scoring system: 0 = 0 to 4 cells stained positive, 1+ = 5 to 10 cells, 2+ = 11 to 50 cells, 3+ = 51 to 200 cells and 4+ >200 cells stained positive per low-power field.

Reverse transcription real-time polymerase chain reaction (RT-PCR)

Total RNA was isolated from the kidney using TRI reagent (Sigma-Aldrich) following a standard protocol (1). Briefly, frozen tissue was cut into small pieces and homogenized in 800 µL TRI Reagent using a needle and a syringe. Next, 200 µL Chloroform were added, samples were mixed and incubated for 8 minutes at room temperature and subsequently centrifuged for 15 minutes at 1200xg at 4°C. The obtained transparent supernatant was transferred in new microcentrifuge tubes and incubated for eight minutes with isopropanol. After the following centrifugation step (1200xg, 4°C, RT), 1 mL ethanol was added and samples were centrifuged for five minutes at 7000xg. Finally, supernatant was discarded, and 500 µL of ethanol were added to each sample. Then samples were centrifuged for five minutes at 7000xg. Thereafter, ethanol was completely removed and the pellet was dissolved in 20 µL dH_2O. The isolated RNA was stored at -20°C.

For the cDNA synthetization a Superscript III Transcription Kit (Invitrogen, Carlsbad, CA, USA) was used (1). 2 µg of total RNA were incubated with 1 µL 10mM dNTPs, 0.5 µL random primers (Invitrogen) and dH_2O for five minutes at 65°C. Next, samples were put on ice and 7 µL mastermix, containing of 4 µL 5x First-Standard Puffer, 1 µL DTT, 1 µL RNaseOUT recombinant RNase Inhibitor and 1 µL SuperScript III reverse transcriptase, were added to each sample. Subsequently samples were put in a thermocycler and incubated for five minutes at 25°C, followed by 45 minutes at 50°C and 15 minutes at 70°C. Obtained cDNA was dissolved in 150 µL dH_2O and stored at -20°C.

Next, real-time PCR was performed in duplicates on a CF96 real-time detection system (BioRad, Vienna, Austria) (1). *Hprt* gene served as house-keeping control and was assessed using SYBR green Master Mix (Invitrogen) and the following primers: forward 5' GCT TCC TCC TCAGAC CGG TTT TTG C 3'; reverse 5' ATC GCT AAT CAC GAC GCT GGG ACT G 3'.

For quantification of mRNA levels, TaqMan gene expression assays (Applied Biosystem, Foster City, DA, USA) were used for *Foxp3* (Mm00475162_m1), *Gata3* (Mm00484683_m1), *Rorc* (Mm01261022), *Tnfa* (Mm00443258_m1), *Tbx21* (Mm00450960), *Ccr2* (Mm00438270), and *CCr5* (Mm01216171). The data was evaluated using $2^{-\Delta\Delta}$ CT method (1).

Measurement of the Glomerular Filtration Rate (GFR)

In order to determine the glomerular filtration rate, a FITC-inulin clearance was performed (1, 93). Shortly, FITC-inulin (Sigma-Aldrich) was weighed to prepare a 5% solution and dissolved in 0.85% NaCl by heating to 90°C. Next, dissolved FITC-inulin was filled into a dialysis membrane and dialyzed for 24 h against 0.85% NaCl. The dialyzed FITC-inulin was sterilized and injected intravenously (2 µL/g body weight). Blood from the tail vein was collected in microcentrifuge tubes filled with Na-Heparin at 3, 5, 7, 10, 15, 35, 56 and 75 minutes after injection. Thereafter, blood samples were centrifuged and obtained plasma was diluted 1:10 in 0.5 mol/L HEPES. For the standard curve, blood from mice of the same background strain was collected in Na-Heparin tubes and diluted 1:10 with 0.5 mol/L HEPES. In order to get standard dilutions from 1:10 to 1:100.000, FITC-inulin solution was diluted with diluted mouse-plasma. The fluorescence of samples as well as of standards were measured using a photometer (FLUOstar Omega Photometer, BMG Labtech, Ortenberg, Germany). Data were analyzed using a two-phase exponential decay function. GFR was calculated using the following equation:

$$GFR = \frac{n}{\frac{A}{K1}+\frac{B}{K2}}, \text{ where}$$

$$n = injected\ amount; n = c * V$$
$$A = Span1; y - intercept\ of\ elimination$$
$$K1 = decay\ constant\ for\ elimination$$
$$B = Span2; y - intercept\ of\ distribution$$
$$K2 = decay\ constant\ for\ distribution$$

Mouse Echocardiography

To investigate cardiovascular changes a transthoracic echocardiography was performed using a VS-VEVO 770 High-Resolution Imaging System (Visualsonics, Toronto, Canada) equipped with a 30MHz RMV (Real-time microvisualization) scan head. (1, 94). 2D-guided M-mode echoes (30 MHz transducer) were recorded from short- and long-axis views at the level of the largest LV-diameter. To ensure spontaneous breathing, mice were lightly anesthetized with 2% isoflurane. Next, the chest was shaved, acoustic coupling gel was applied and, to avoid hypothermia, a warming pad was used. Then mice were imaged in a left lateral decubitus position. LV end-diastolic (LVEDD) and end-systolic (LVESD) were averaged from three consecutive cardiac cycles as recommended by the leading-edge convention of the American Society of Echocardiography. Fractional shortening was calculated using following equation (94):

$$100x((LVEDD - \frac{LVESD}{LVEDD})$$

Statistical analyses

Statistical analyses were performed using GraphPad Prism 6.0 (GraphPad Software, La Jolla, CA, USA) and all results from experiments are shown as mean ± SEM. Testing for normal distribution was done using the Kolmogorov-Smirnov test with Dallal-Wilkinson-Lilliefors correction. Differences between two groups were compared by either nonparametric Mann-Whitney U-test or unpaired Student's t-test according to the distribution. When comparing the three groups, ANOVA or Kruskal-Wallis test was performed with subsequent Dunn's test with adjustment for multiple comparisons. A two-tailed $p<0.05$ was considered statistically significant (1).

Results – Findings

DBA/2 mice on high-phosphate diet develop Chronic Kidney Disease

Female DBA/2 mice were set on high-phosphate diet for either 4 (HPD4) or 7 (HPD4) days with subsequent return to standard chow diet. Mice were followed up until day 84. DBA/2 mice from control groups were fed with standard chow diet (SCD) for the complete time of the experiments. After 84 days, all mice subjected to the HPD displayed a remarkable phenotype of nephrocalcinosis. Histopathological evaluations with Alizarin Red staining of the kidneys revealed that HPD mice compared to SCD mice developed phosphate nephropathy with tubular calcium hydroxyapatite crystal (Figure 2A). Kidneys of SCD groups showed only small and significantly fewer alizarin red positive deposits. In order to determine renal fibrosis a Picrosirius red staining was performed. In all kidneys of HPD mice fibrotic areas, particularly in the peritubular region, were found (Figure 2A). Of note, glomeruli were not affected by fibrosis. As expected, an increased histological phenotype was observed in HPD7 mice when compared with HPD4 mice (1).

To determine if mice have developed chronic kidney disease, kidney function was quantified using FITC-inulin clearance. Mice fed high phosphate diet revealed decreased glomerular filtration rate (GFR) when compared to SCD group. However, only HPD7 mice had a significantly decreased GFR in comparison to mice from SCD group (Figure 2B, C). Additionally, serum urea levels were elevated in both HPD groups as compared to SCD group (Figure 2D) (1).

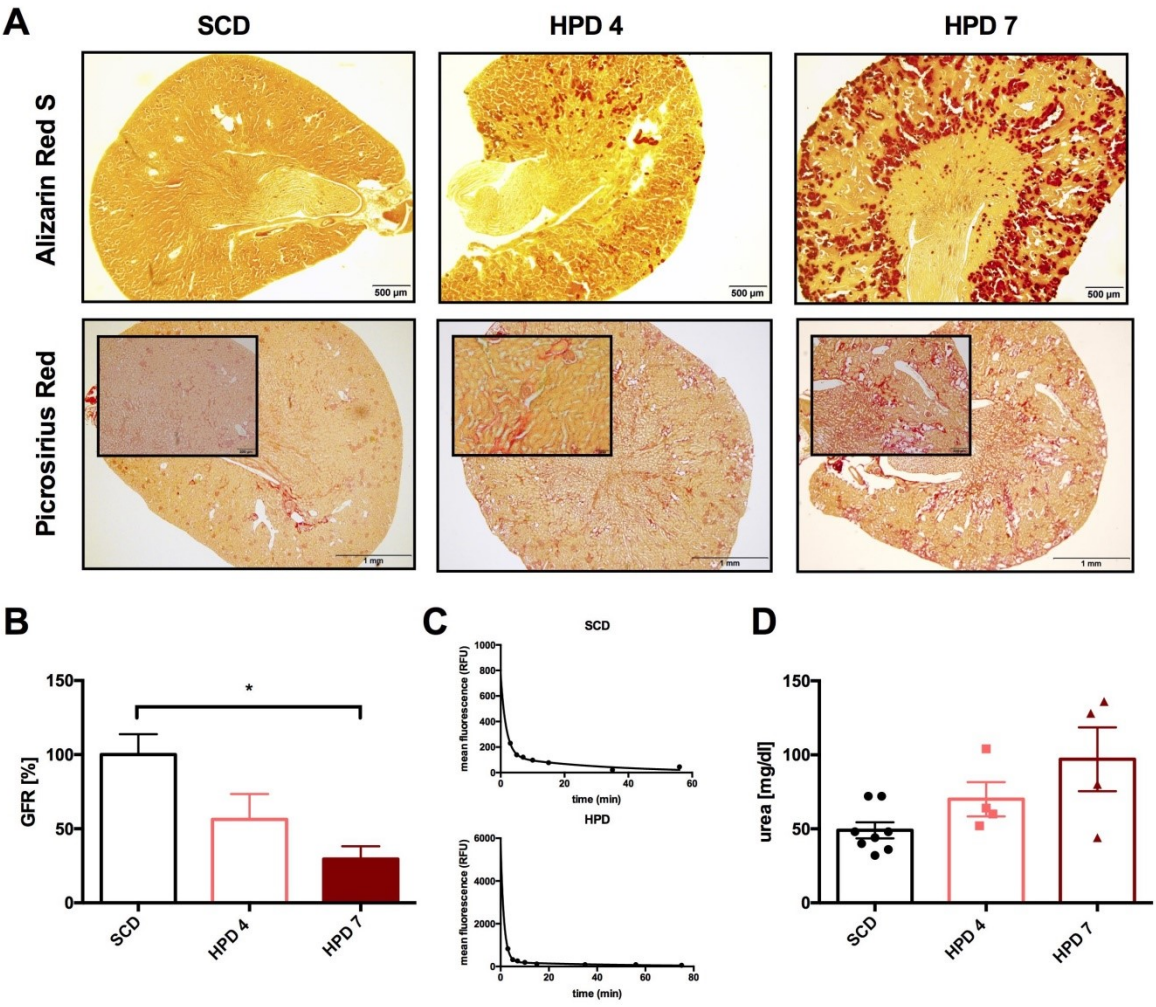

Figure 2: The impact of high phosphate diet on renal phenotype

Female DBA/2 mice were either fed with HPD for 4 (HPD4, n=4, light red bars) or 7 days (HPD7, n=4, red bars) and subsequently set on SCD and followed up on day 84. Mice only fed standard chow (SCD, n=8, black bars) served as control group. Histopathological evaluation with Alizarin Red staining (A, upper panel) showed a remarkable renal calcification in both HPD groups compared with the SCD group. Picrosirius red staining (A, lower panel) revealed fibrosis in the peritubular areas in kidneys of mice fed HPD. Representative pictures with 40X magnification are provided. GFR levels (B) were upregulated in the HPD4 group and were significantly higher in the HPD7 group as compared to the SCD group. Representative GFR curves of SCD and HPD 7 mice are shown (C). Furthermore, serum urea was increased in both HPD groups (D). * $p<0.05$
This figure has been published previously in (1).

Immunohistochemical staining of kidneys further revealed a significant increase of infiltrating $CD4^+$ and $CD8^+$ T cells in HPD mice compared with SCD mice (Figure 3A). However, $CD68^+$ macrophages constituted the major infiltrating cell population in HPD treated mice (Figure 3B).

Macrophages were mainly present in the cortico-medullar border zone (Figure 3C), where calcium-phosphate precipitations occurred (1). These findings were confirmed by qPCR (Figure 3D). mRNA levels of macrophage markers such as chemokine receptors *CCr2* and *CCr5* were increased in mice fed HPD as compared to SCD mice. Additionally, HPD mice had higher mRNA levels of *Tnfa* and *Foxp3* than mice from control group. Gene expression levels of *Tbx21*, *Gata3*, and *Rorc* were similar between groups (1).

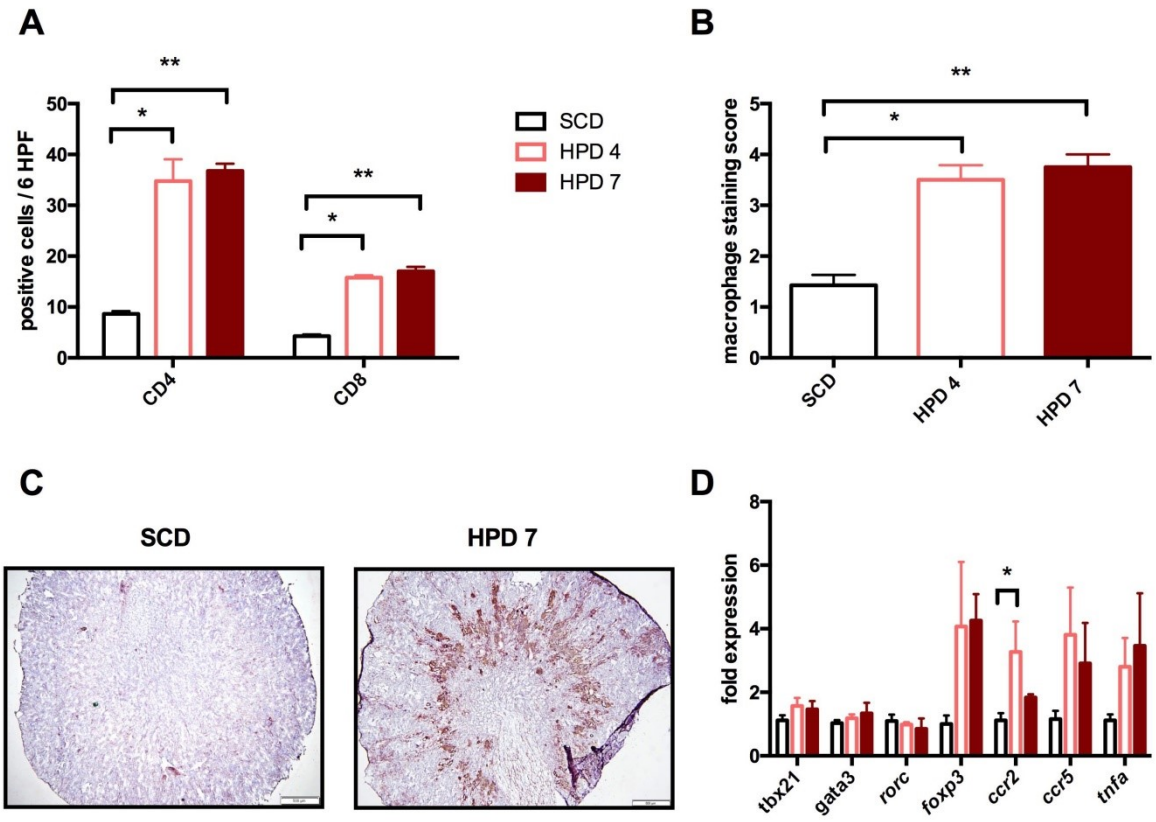

Figure 3: Inflammatory Phenotype of Kidney

Renal sections of HPD- and SCD-fed mice were stained for infiltrating leukocytes (SCD: n=8, black bars; HPD4: n=4, light red bars; HPD7: n=4, red bars). Quantification of kidney infiltrating $CD4^+$ and $CD8^+$ T cells as well as $CD68^+$ macrophages (B) was performed on immunohistochemically stained kidney sections from mice from HPD4, HPD7 and SCD group. Representative pictures of $CD68^+$ stained renal tissue from SCD and HPD7 mice are provided (C). qPCR for macrophage markers, TH1, TH2 and TH17 markers was performed (D). Data are presented as mean ± SEM. Magnification for C is x40.

* $p<0.05$, ** $p<0.01$

This figure has been published previously in (1).

Cardiovascular changes in chronic kidney-diseased DBA/2 mice

One of the most frequent complications of chronic kidney disease are cardiovascular diseases (74). To evaluate the heart phenotype, echocardiography of HPD7 mice and of SCD mice was performed before starting the HPD treatment and additionally on day 84, at the end of the experimental setup (1). Due to the fact that on day 84 in HPD7 group the n-number (n=2) was small, the echocardiographic assessment should be considered to have a major limitation. Nevertheless, no difference in left ventricle systolic function (EF and FS) was observed between the two groups on day 84 (Figure 4A, B). Though, left ventricle mass tended to be elevated in HPD7 mice in comparison to SCD mice (Figure 4C). Heart weights (Figure 4D) were similar in both groups (1).

Alizarin Red staining was performed to analyze the abdominal aortas for calcification (Figure 4E). Calcified areas were found in HPD7 mice, whereas no histopathological signs of calcification in SCD mice were detected (1).

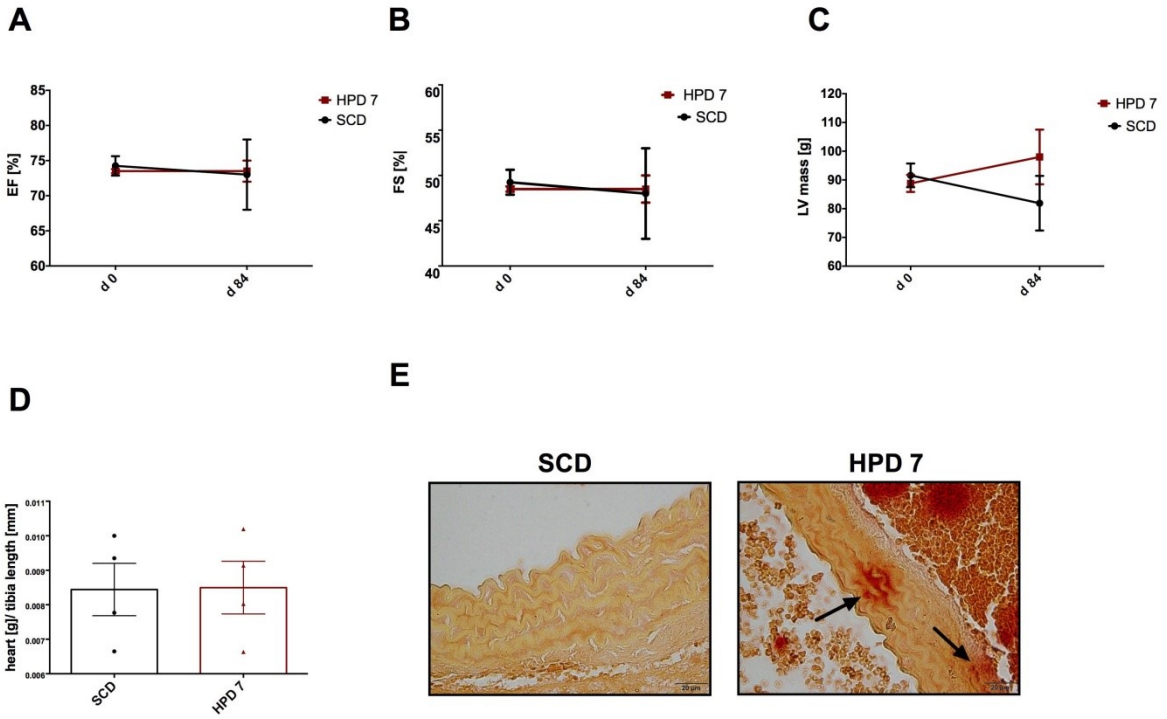

Figure 4: Cardiovascular phenotype in DBA2/mice

Echocardiographic evaluations of mice in HPD7 and in SCD group were performed before starting HPD treatment (SCD: n=4, black line; HPD n=4, red line) as well as on day 84 (SCD: n=4, black line; HPD: n=2, red line). Quantification of EF (A) and FS (B) was done. LV mass (C) and heart weight (D) was determined. Aortic calcification (E) was visualized by Alizarin red staining. Data are shown as mean ± SEM. Magnification for E is x200.
This figure has been published previously in (1).

Development of a low-turnover bone disease in chronic kidney-diseased DBA/2 mice

Since, that chronic kidney disease is often accompanied by a disturbed mineral and bone metabolism, we next investigated the bone phenotype of mice fed high phosphate diet.
First, parathyroid (Pth) and fibroblast growth factor 23 (Fgf-23), both key regulators in mineral and bone metabolism, were measured. Evaluation of Fgf-23 levels did not differ between the three groups. Though, Pth levels were significantly increased in HPD7 mice as compared to SCD mice (1).

To evaluate the bone structure, mice were calcein-labelled and tibias were analyzed by bone histomorphometry on day 84. Analysis of bone volume/tissue volume (BV/TV), mineral apposition rate (MAR) as well as bone formation rate (BFR) revealed significant decreased levels in HPD7 mice when compared with SCD mice. Furthermore, the HPD treatment resulted in a significant decrease in bone formation rate (BFR), eroded surface/bone surface (ES/BS), osteoid surface/bone surface (OS/BS), and trabecular thickness (Tb.Th). No difference between groups was detected in trabecular separation (Tb.Sp) and trabecular number (Tb.N). These static and dynamic histomorphometry results lead to the assumption, that the mice have developed a low-turnover bone disease. The bone phenotype was more pronounced in HPD7 mice as compared to HPD4 mice, though (1).

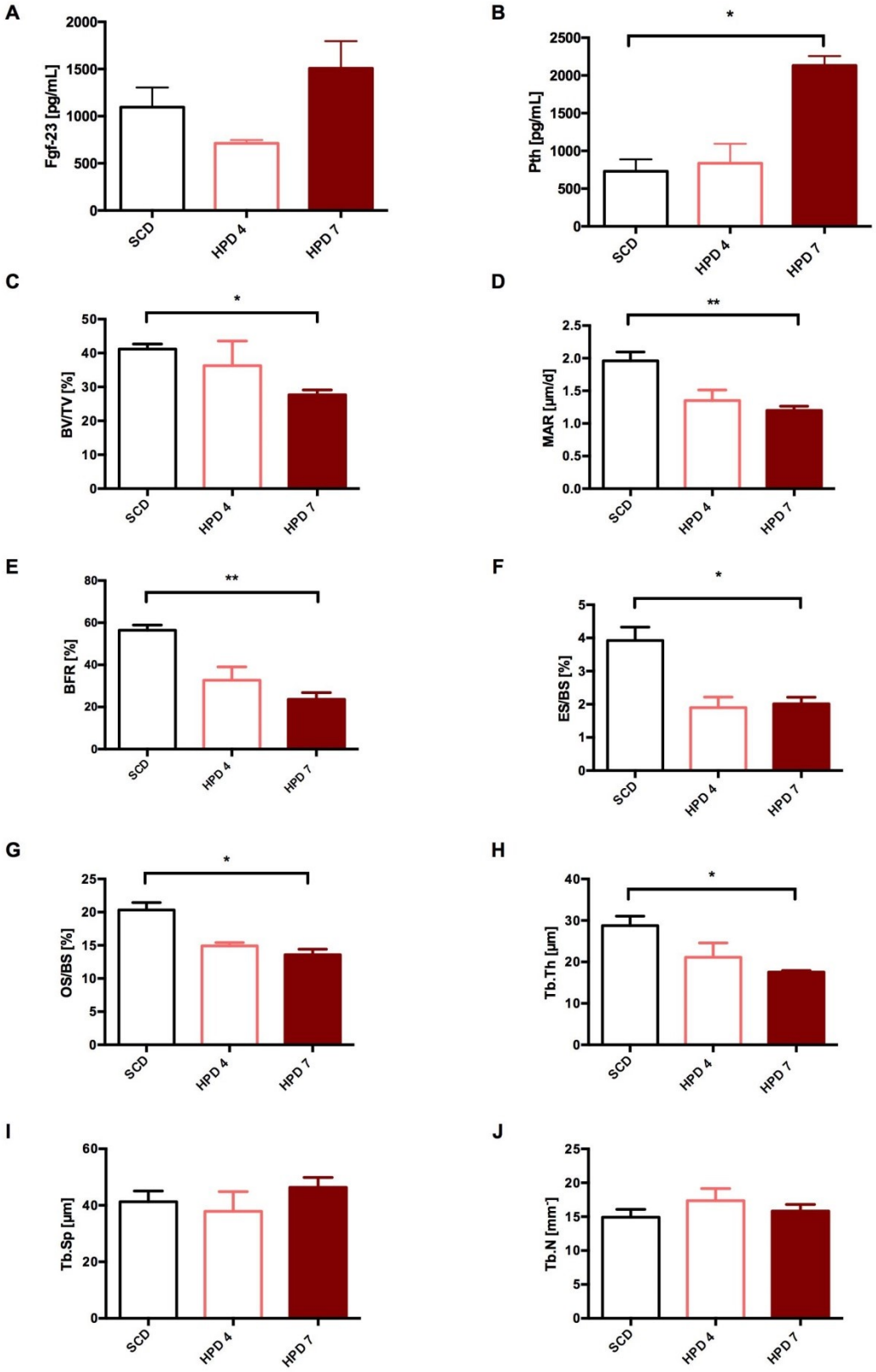

Figure 5: DBA/2 mice developed low-turnover bone disease

The mineral and bone metabolism of HPD7 (n=4; red bars), HPD4 (n=4, light red bars) and SCD mice (n=8; black bars) was evaluated on day 84. Serum Fgf 23 levels (A) as well

as serum Pth levels (B) were quantified. Bone structure was assessed by means of bone hisotomorphometry. Bone volume/tissue volume (BV/TV; C), mineral apposition rate (MAR; D), bone formation rate (BFR; E), eroded surface/bone surface (ES/BS; F), osteoid surface/bone surface (OS/BS; G), trabecular thickness (Tb.Th; H), trabecular separation (Tb. Sp.; I) as well as trabecular number (Tb.N.; J) are shown. Data are shown as mean ± SEM. * $p<0.05$, ** $p<0.01$

This figure has been published previously in (1).

Part B - Autophagy protects from uremic vascular calcification

Introduction

Chronic kidney disease is known to be a worldwide health concern and is associated with high rates of morbidity, mortality and healthcare expenditure (13). One of the most frequent complications of CKD is an abnormal mineral metabolism resulting in cardiovascular diseases. Thus, patients suffering from chronic kidneys disease, especially end-stage renal disease (ESRD), have a high burden of cardiovascular morbidity and mortality (13). Cardiovascular mortality in dialysis patients is 10 to 20 times higher than in the general population (95). Characteristically, vascular change in patients with CKD as well as ESRD is accompanied by reduced vascular compliance, left ventricle hypertrophy as well as vascular calcification (71).

As already described in the introduction section of *Part A* of the present thesis, patients suffering from CKD are predominantly affected by calcification of the *tunica media*, whereas non-uremic patients are prone to develop arterial calcification marked by intimal atherosclerotic plaques (73).
However, not only patients with CKD and secondary hyperparathyroidism develop calcification of the *tunica media*, but also patients with diabetes. Monckeberg's media sclerosis is the most common type of media calcification and frequently associated with long-standing diabetes mellitus. Monckeberg's media sclerosis is often localized in the arteries of the extremities (96). Media calcification was already described a century ago, but still the pathogenesis is not fully understood (96-98). Hyperglycaemia as well as disorders in calcium and phosphate homeostasis causes media calcification. Its common patients with advanced CKD and ESRD display elevated levels of serum phosphate and increased total body calcium (99, 100). Hence, the current state of research indicates that hyperphosphatemia is the main cause for developing media calcification (101). Nevertheless, the underlying mechanism to explain the pathogenesis of media calcification is more complex. Thus, uremic media calcification is not only driven by systemic factors such as increased serum phosphate levels or hyperglycaemia but is itself also dependent on vascular smooth muscle cells (VSMCs). Increased levels of serum phosphate in

combination with other serum mediators, which are imbalanced in uremia, result in the transdifferentiation of VSMCs from a contractile to proliferative, osteoblastic, and/or inflammatory phenotype. That is possible because VSMCs are not terminally differentiated cells and thus able to react to stress or injury by transdifferentiating (102-105).
Of note, high levels of serum phosphate are not only a risk factor for cardiovascular diseases such as vascular calcification in patients with advanced stages of CKD, but also for patients suffering from moderate CKD as well as in the general population (106-108).

To study the vascular outcomes in CKD a few animal models were employed in the last years (109). Previous data from our group showed that it is also possible to use DBA/2 mice, which develop phosphate nephropathy when subjected to HPD due to their alternative splice variant of the *Abcc6* gene (88, 110, 111). During a period of 5-14 days mice developed calcification of the *tunica media* in aortas, which was more pronounced in the abdominal aorta than in the thoracic part of the aorta. This calcification pattern reflects the situation in patients suffering from ESRD (111). Additionally, the data revealed that immune cells play an important role in the development of renal calcification (110), while uremic vascular media calcification is not accompanied by inflammatory processes (111).

In the last years a growing interest in the role of autophagy in vascular biology has evolved as well as an increasing suspicion that autophagy influences the vascular pathophysiology including uremic vascular media calcification (112). Autophagy is generally differentiated in three types, called microautophagy, chaperone-mediated and macroautophagy (112, 113). In our experimental setup we focused on macroautophagy, hereafter referred to as autophagy.
Autophagy is an evolutionarily highly conserved cellular process which is involved in the degradation of long-lived cytosolic proteins and organelles. Autophagy is not only a survival response to stress, but also important for cellular and organismal homeostasis. Hence, dysfunction or dysregulation of autophagy often result in various disease (114, 115).

Furthermore, autophagy is a dynamic process, consisting of several sequential steps, including the formation and fusion of membrane compartments. To explore and observe this complex autophagic mechanism, different protein markers can be used (62, 116). One of the most common used markers is microtubule-associated protein light chain 3 (LC3).

Two forms of LC3, namely LC3-I and LC3-II, exist in various cells. During the autophagic process the cytosolic LC3-I converts to the membrane bound LC3-II. Due to that LC3 specifically binds to the membranes of autophagosomes, an increased accumulation of LC3-II is proportional to the extent of autophagosome formation (62). Another marker for detecting autophagy is the p62 protein. It is also named sequestome 1 (SQSTM 1) and is a ubiquitin-binding scaffold protein which is degraded by the autophagic process. Thus, low protein levels of p62 indicate that an autophagic process is taking place in cells (117).

We now aimed to characterize the role of autophagy in uremic vascular media calcification induced by high-phosphate treatment *in vivo* as well as *in vitro (2).* Recently, *Dai et al.* showed *in vitro* that high-phosphate levels result in an increase of radical oxygen species (ROS) which leads to augmented autophagy in VSMC. Thus, cells were protected from calcification by autophagy counteracting phosphate induced vascular calcification due to the reduction of matrix vesicle release (118).
However, experimental studies of pharmacologically-induced autophagy to ameliorate uremic vascular media calcification *in vivo* are rare. *Peng et al.* revealed that the calcification process of aortas is influenced by autophagy, but they did not use a chronic kidney disease model to investigate the aortic calcification (119).

Together, these data underline the need for further research to investigate the role of autophagy in uremic vascular media calcification in order to improve the cardiovascular burden in patients with CKD and ESRD. Hence, we described the role of autophagy in uremic media calcification in a murine as well as in a cellular model. Furthermore, we influenced autophagy pharmacologically and studied the effects on uremic media calcification (2).

Material and Methods

Study design

For *in vivo* studies female 8-week-old DBA/2 mice were obtained from Charles River (Sulzfeld, Germany) and kept in a virus- and antibody-free environment in the laboratory animal facility. These mice develop renal as well as media calcification when fed with high phosphate diet (88, 89). To induce media calcification, mice were set on high phosphate diet (Altromin, Germany), containing 20.2 g of phosphorus, 9.4 g of calcium, 0.7 g of magnesium and 500 IU/kg of vitamin D3. The control group received standard chow diet, containing 7,0 g of phosphorus, 10.0 g of calcium, 2.2 g of magnesium and 1000 IU/kg of vitamin D3. To investigate the effect of autophagy on vascular calcification, mice were treated with rapamycin (LC labs, Woburn, MA, USA). For this purpose rapamycin was dissolved in 100% ethanol, which was then diluted with sterile saline for intraperitoneal injection at a dose of 0.5 mg/kg body weight. Mice were injected daily, starting either 3 days prior to or 5 days after beginning the high phosphate diet. Then, mice were followed up for 5 and 12 days (2).
All animal experiments were approved by the Committee of the Ethics of Animal Experiments of the Austrian Ministry (BMWFW-66.010/0061-WF/V/3b/2016). All experiments were conducted under strict adherence to Austrian law.

For in vitro studies mouse vascular smooth muscle cells (MOVAS) were obtained from the American Type Culture Collection (ATCC, Manassas, VA, USA). Cells were maintained in high glucose Dulbecco's Modified Eagle's Medium (ATCC) supplemented with 10% FCS (Gibco, Life Technology, Vienna, Austria) and an antibiotic mixture of 1% penicillin/streptomycin. Cells were seeded in six-well plates at a density of 1.0 X 10^4 cells/cm^2. To induce calcification, the medium was supplemented with either 1.25 mM β-glycerophosphate (βGP) (Sigma Aldrich, St. Louis, MO, USA) and 25 µg/mL ascorbic acid (AA) (Sigma-Aldrich) or with 2.5 mM β-GP and 50 µg/mL AA, and cells were kept for 7, 14 or 21 days (2, 120, 121).

To induce autophagy, cells were treated with 10 µM rapamycin (LC labs). To investigate the effect of inhibited autophagy, cells were exposed either to 5 mM 3-methyladenine (3-MA) (Sigma Aldrich) or to 20 nM bafilomycin A1 (Sigma Aldrich). To determine the autophagic flux on day 21, cells were exposed to 50 nM bafilomycin A1 for 3 h before harvesting.
Incubation was performed at 37°C in a humified, 5% CO_2 atmosphere and the medium was changed every other day (2, 120).

Evaluation of biochemical analysis

Blood urea nitrogen levels were evaluated using a colorimetric detection kit (Thermo Fisher Scientific) following the manufacturer's instructions (2, 120).
To quantify the calcium levels of aortas and kidneys a Calcium Detection Assay Kit (Abcam) according to the manufacturer's instructions was used and calcium content was normalized to tissue weight. To determine the calcium content in MOVAS, cells were decalcified with 0.6 M HCl and the calcium content in supernatants was measured using the Calcium Detection Assay Kit (Abcam) following the manufacture's instruction. The calcium levels were normalized to the protein content, which was quantified using the PierceTM BCA Protein Assay Kit (Thermo Scientific) following the manufacturer's instructions (2, 120).
Calcium deposition was visualized by staining MOVAS with Alizarin Red S (Sigma-Aldrich). Briefly, cells were washed with PBS, fixed in 4 % formalin for 15 minutes and incubated for 10 minutes with 2% Alizarin Red S solution at room temperature. Finally, cells were washed 5 times with dH_2O. To quantify stained cells, MOVAS were extracted with 10% cetylpyridium chloride (Sigma-Aldrich) for 10 min. The OD was measured at 570 nm on a FLUOstar Omega photometer (BMG Labtech, Ortenberg Germany) (2, 120).

Reverse Transcription Real-Time Polymerase Chain Reaction

Real-time PCR for *Trp53in*, *Igfbp3*, *Hmox1*, *Adrb2*, *Atg16l1* and *Il-1beta* was performed to evaluate autophagy related genes. To investigate the role of inflammation, real-time PCR for *Tnf*- α, *Tbx21*, *Il-6* and *Foxp3* was done. mRNA levels of *Sm22*-α and *Runx2* were

determined to evaluate the effect of autophagy on osteoblastic differentiation either *in vitro* or *in vivo* (2, 120).

Murine tissue and cells were stored at -80°C before RNA was isolated using AllPrep®DNA/ RNA/Protein Mini Kit (Qiagen, Venlo, Netherlands) according to the manufacturer's instructions. To obtain cDNA, 100 ng of total RNA was reverse-transcribed using Superscript III Transcription Kit (Invitrogen) and random primers (Invitrogen). Next, qPCR was performed in duplicates on a CFX96 a CFX96 Real-Time System (BioRad). For quantification of respective genes, TaqMan gene expression assays (Applied Biosystems) for *Trp53in* (Mm00458142_g1), *Igfbp3* (Mm01187817_m1), *Hmox1* (Mm00516005-m1), *Adrb2* (Mm02524224_s1), *Atg16l1* (Mm00513085_m1), *Il-1beta* (Mm00434228_m1), *Tnf-alpha* (Mm00443258_m1), *Tbx21* (Mm00450960_m1), *Il-6* (Mm00446190_m1), *Foxp3* (Mm00475162_m1), and *Sm22*-α (Mm00441661_g1) were used. For *Runx2* SYBR green (Invitrogen) was assessed using the following primers: forward 5′TCC TAT CTG AGC CAG ATG ACA TCC 3′ and reverse 5′CCG GTC TCC CCC GGG TAC C 3'. *Hprt* served as a reference gene and was assessed using SYBR Green Mastermix (Invitrogen) with the following primers: forward 5′GCT TCC TCC TCA GAC CGC TTT TTG C 3′ _and reverse 5′ATC GCT AAT CAC GAC GCT GGG ACT G 3′. Data were calculated using $2^{-\Delta\Delta}$ CT method (2).

Western Blot analysis

Protein was isolated by sonicating aortic tissue and cells in a homogenization buffer (0.25 mol/L sucrose, 10mmol/L HEPES, pH 7.5 and 1mmol/L EDTA, pH 8.0) containing HALTTM Protease Inhibitor Cocktail, EDTA-free (Thermo Fisher Scientific, Rockford, USA) (2). Thereafter, isolated protein was quantified with PierceTM BCA Protein Assay Kit (Thermo Fisher Scientific) strictly following the manufactures' instruction. Aliquots of total protein were separated using a 12% sodium dodecyl sulfate polyacrylamide gel electrophoresis (SDS-PAGE) for 1.5-2 hours at 100V. Next, proteins were transferred to polyvinylidene fluoride (PVDF) membranes (Merck Millipore, Burlington, Massachusetts, USA) for 90 min at 150 mA. Subsequently, membranes were blocked in 5% nonfat dry milk diluted in TBS-Tween for 3h at room temperature, followed by incubation with primary antibodies against GAPDH (Cell Signalling, Cambridge, UK), p62 (Abcam, Cambridge, UK) and LC3 (Novus Biologicals Littleton, Colorado, USA) overnight at 4°C.

After three washing steps in 5% nonfat dry milk/TBS-Tween, blots were washed once in TBS-Tween and the appropriate HRP-conjugated secondary antibody (Cell Signalling) was applied for one hour at room temperature. After another washing step with TBS-Tween, protein signals were visualized using PierceTM ECL Western Blotting Substrate (Thermo Fisher Scientific) and a ChemiDoc System (BioRad). Densitometric analysis were performed using Image Lab software (BioRad) (2).

Histological Evaluation

Aortas and kidneys of DBA/2 mice were isolated and placed in 4% formalin for two days for fixation (2). Next, tissue was dehydrated in graded ethanol and embedded in paraffin. For staining, aortas as well as kidneys were cut in 4 µm sections on a rotation microtome.

To visualize the amount of media calcification Alizarin Red S staining was done by immersing deparaffinized samples in 2% Alizarin Red S solution (Sigma Aldrich) subsequently by rinsing in acetone and acetone xylene (2).

A three-layer immunoperoxidase staining technique was used for the assessment of LC3 in aortas. Shortly, tissue sections were treated with standardized heat-mediated antigen retrieval in an automated de-cloaking chamber (Aptum, Southampton, UK) and subsequently quenched in 0.3% H_2O_2 diluted in methanol. Next, slides were blocked with biotin/avidin blocking kit (Vector Laboratories) and incubated with a rabbit-derived primary antibody against LC3 (Novus Biologicals) at 4°C overnight. Finally, a biotin-conjugated goat anti-rabbit IgG (Jackson ImmunoResearch Laboratories, West Grove, PA, USA) was used as a secondary antibody (2).

To detect ROS production in aortas, nitro blue tetrazolium (NBT) staining was performed. Briefly, rehydrated paraffin samples were washed in HBSS and incubated with NBT diluted in HBSS (1.6 mg/mL) at 37°C for 20 minutes (2).

In order to evaluate the renal pathology, Periodic-Acid-Schiff (PAS) staining was done. For this purpose, dehydrated kidney slides were incubated in Periodic Acid Solution (Sigma-Aldrich) for 5 minutes, followed by rinsing in dH_2O. Next, slides were immersed in Schiff's Reagent (Sigma-Aldrich) for 15 minutes with subsequent washing in running tap water. Finally, slides were counterstained in Gill's Hematoxylin (Sigma-Aldrich) (2).

Immunofluorescence

In order to evaluate the impact of autophagy on differentiation of MOVAS, aSMA expression was detected using immunofluorescence staining. Thus, MOVAS were grown on glass chamber slides and fixed in 4% paraformaldehyde for 20 minutes at room temperature. Next, cells were permeabilized with 100% ice-cold methanol and rinsed with PBS and washing buffer (0.1% BSA/PBS) with subsequent incubation with blocking buffer for 45 minutes. After another washing step, slides were incubated with the primary antibody rabbit-anti-α-smooth muscle actin (Sigma-Aldrich) for 1h at room temperature. Thereafter, slides were extensively washed and a FITC-conjugated secondary antibody was applied for 1 h at room temperature. Finally, slides were mounted in ProLong Gold anti-fade with DAPI (Thermo Fisher Scientific), sealed with nail polish and stored at 4°C. Evaluation was done using a LSM510 META (Zeiss, Oberkochen, Germany) (2).

Statistical Analyses

Results from all experiments are presented as mean ± SEM. Normal distribution of data were assessed by the Kolmogorov-Smirnov test with Dallal–Wilkinson–Lillifors correction. Two groups were compared by either nonparametric Mann-Whitney U test or unpaired t test as appropriate, depending on the distribution of the variable in question. When comparing three or more groups, ANOVA or Kruskal–Wallis test was performed with subsequent Dunn's test with adjustment for multiple comparisons. Differences in mortality rates between rapamycin and vehicle-treated mice were assessed by the Kaplan–Meier method and log-rank (Mantel-Cox) test. A two-sided $p < 0.05$ was considered statistically significant. All statistical analysis were done using GraphPad Prism 6.0 for Macintosh (GraphPad Software, La Jolla, CA, USA) (2).

Results – Findings

Induction of autophagy in aortic vascular smooth muscle cells in DBA/2 mice

Previous data shows that DBA/2 mice develop uremic media calcification as wells as renal calcification when treated with HPD (110, 111). To confirm these results in our experimental setup, we determined the amount of calcium in kidneys and measured BUN levels (2). DBA/2 mice subjected to high phosphate diet for 5 (HPD 5d) or 12 (HPD 12d) days showed significantly higher calcium contents in the kidneys in comparison to mice fed with standard chow diet (SCD) treated mice (Figure 6A). Furthermore, the blood urea nitrogen (BUN) levels were significantly increased in mice treated with HPD for 12 days (Figure 6B).

Previously a microchip array was performed in our lab and revealed that autophagy pathway-associated genes are regulated in DBA/2 mice fed high phosphate diet (111). Thus, an increase of mRNA levels of *Trp53in* and *Igfbp3* in aortas of DBA/2 mice treated with HPD for 5 or 14 days have already been shown (111). We could confirm these findings (Figure 6C) and both autophagy related genes, *Trp53in* and *Igfbp3*, were upregulated in aortas of DBA/2 set on HPD for 5 or 12 days (2). Additionally, we evaluated other autophagy-associated genes, such as *Hmox1*, *Adrb2*, and *Atg16l1* and a significantly increase of mRNA levels was detected. Interestingly, *Il-1beta* was not regulated on a transcriptional level at any time. As expected, the pattern of gene regulation was more pronounced after 12 days of HPD treatment than after 5 days of HPD (2).

Next, to investigate the role of autophagy in the calcifying process of aortas in DBA/2 mice, Western Blot analysis was performed. LC3-II and p62, both protein markers of autophagy, were quantified for aortas in DBA/2 mice subjected to HPD for 5 or 12 days. LC3-II levels (Figure 6D) were significantly increased and accordingly p62 levels (Figure 6E) were significantly decreased in 12 days treated HPD mice when compared with controls on standard chow diet (2).

To confirm previous results showing that DBA/2 mice treated with HPD develop aortic calcification (111), Alizarin Red S staining of aortas was performed. Arterial calcification was found to be located in the *Tunica media* and was more pronounced in DBA/2 mice treated for 12 days with HPD (Figure 6G).

Furthermore, immunohistochemistry staining for LC3-II was performed. The expression of the autophagy marker LC3-II was increased in vascular smooth muscle cells of the *Tunica media* as well as in the vascular endothelial cell layer of mice set on HPD (Figure 6G). Additionally, NBT staining to visualize ROS production in aortic tissue was carried out. Evaluation of NBT staining revealed an elevated production of ROS in the *Tunica media* in 12 days treated HPD mice as compared to SCD mice (Figure 6G) (2).

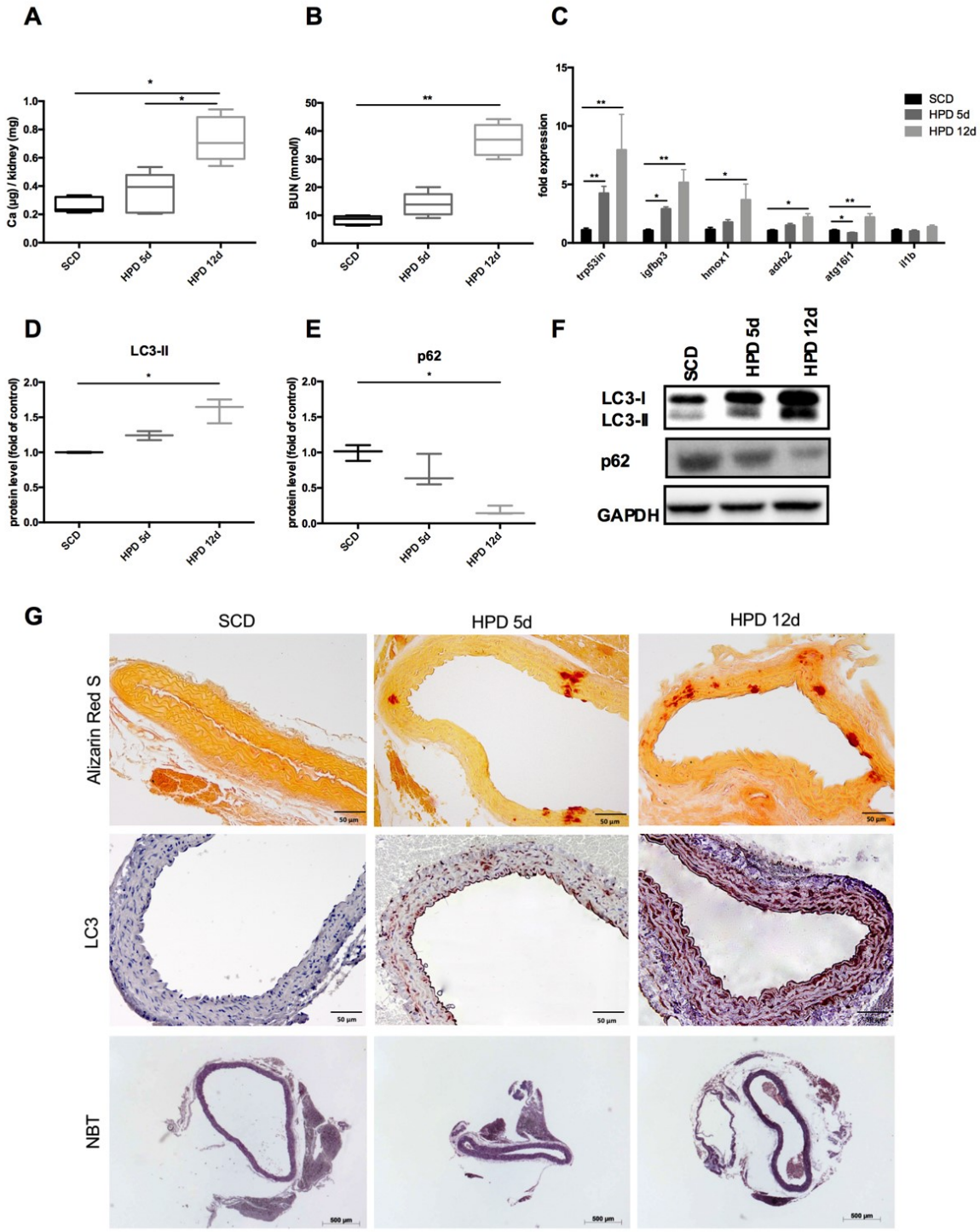

Figure 6: Uremic media calcification in DBA/2 mice cause increase of autophagy

DBA/2 mice were treated with high-phosphate diet (HPD; HPD d5: n= 6; HPD d12: n=4; grey bars) or standard chow diet (SCD; n= 11; black bars) and followed up for 5 or 12 days. Calcium content of kidney (A) as well as BUN levels (B) were determined. Real time PCR for autophagy associated genes (C) was performed.

Protein levels of LC3-II (D) and p62 (E) were analyzed using Western Blot. Three independent experiments were performed. A representative Western Blot (F) is shown. Alizarin Red S staining (G, upper panel) of aortas of SCD- and HPD-fed mice was performed. Stainings of aortic tissue of DBA/2 mice set on SCD or HPD to detect LC3 (G, middle panel) and NBT (G, lower panel) was done. Representative pictures of aortas are provided. All data are presented as mean ± SEM. *$p < 0.05$, **$p < 0.01$.
This figure has been published previously in (2).

Calcification of mouse vascular smooth muscle cells (MOVAS) induces autophagy

Next, we established an *in vitro* model to mimic vascular calcification in vascular smooth muscle cells. Initial studies were performed to determine if calcification in MOVAS occurs when cells are cultured in the presence of a calcifying medium containing ascorbic acid (AA) and β-glycerolphosphate (β-GP). Thus, cells were treated with such medium, which was supplemented with two different concentrations of AA and β-GP, for 7, 14 and 21 days (2).
Alizarin Red S staining intensity in MOVAS cultured under calcifying conditions was increased over time and with a higher concentrated calcification medium (Figure 7A). Additionally, the cellular calcium content (Figure 7B) was proportionally increased with time and higher concentration of the calcifying medium (2).

Then, autophagy related genes were evaluated (Figure 7C-F). On day 14 and 21, mRNA levels of *Trp53in*, *Igfbp3* and *Atg16l1* were significantly increased in MOVAS treated with 2,5mM β-GP and 50µg/mL AA. Gene expression levels of *Hmox1* were significantly upregulated in MOVAS treated with high-phosphate supplementation on day 21 (2).

To gain an insight into the role of autophagy in our *in vitro* model, the protein marker LC3-II and p62 were evaluated. Western Blot analysis revealed a significant increase of LC3-II levels (Figure 7G, I) in MOVAS cultured under high-phosphate calcifying conditions. Accordingly, p62 levels (Figure 7H, I) decreased under identical conditions (2).

To determine if the calcification process is the reason for elevated autophagy levels in MOVAS, autophagic flux was measured (Figure 7J, K). Thus, after 21 days, MOVAS cultured with and without calcifying medium were incubated with bafilomycin for 3h and immediately analyzed for the autophagy marker LC3-II. Increased levels of LC3-II in MOVAS treated with bafilomycin compared to respective controls proved, that the calcification itself increased autophagy in MOVAS (2).

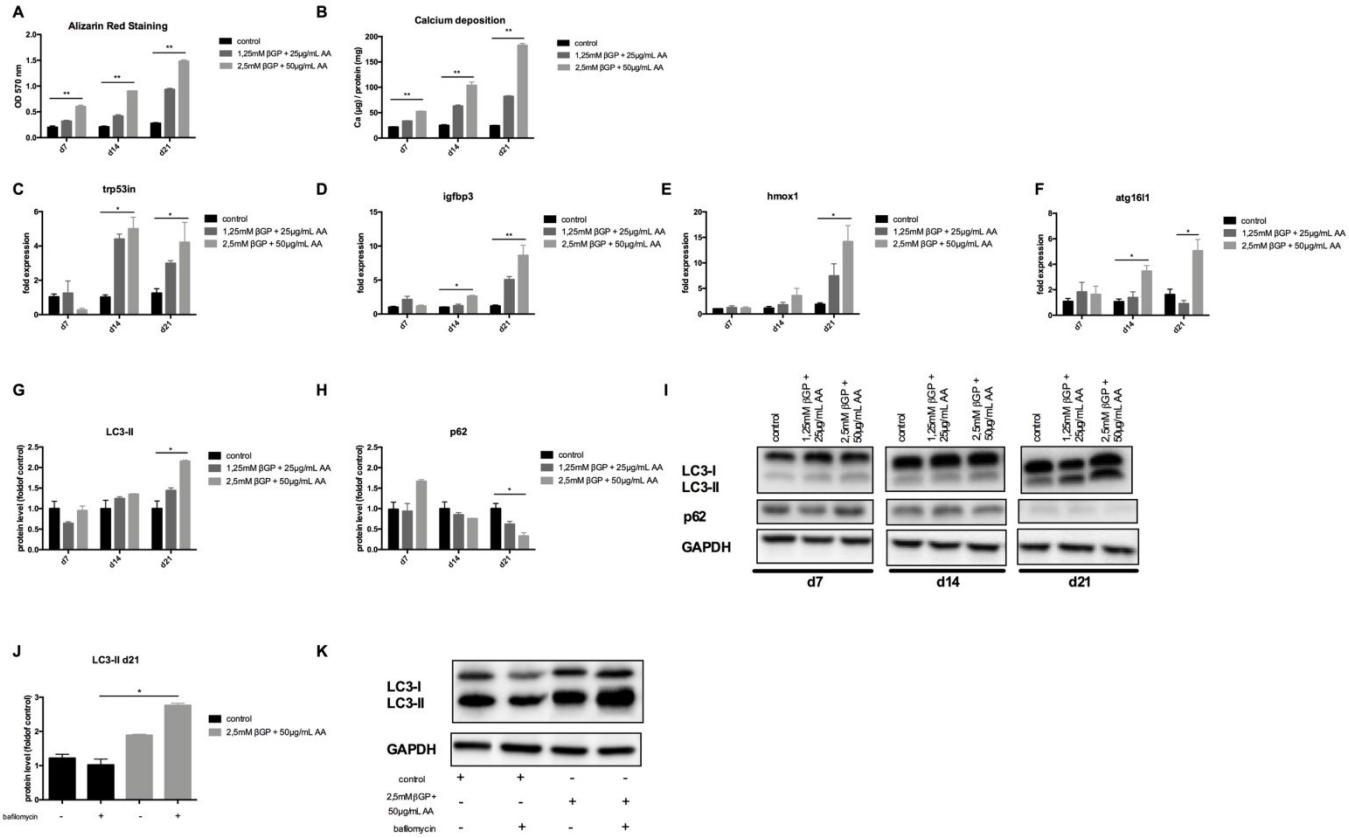

Figure 7: Calcification causes autophagy in MOVAS

MOVAS were cultured in absence (black bars; n=4) or presence of calcifying medium, containing either 1.25 mM βGP and 25 µg/mL AA (light grey bars, n=4) or 2.5 mM βGP and 50 µg/mL AA (grey bars, n=4) for 7, 14 or 21 days. Photometric quantification of Alizarin Red S stained calcium deposition in MOVAS (A) as well as measurement of cellular calcium content (B) was performed. Evaluation of qPCR for autophagy related genes (C-F) was done. Western Blot analysis for determination of LC3-II (G) and p62 (F) was performed. Three independent experiments were done. A representative Western Blot (I) is provided. The autophagic flux (J) was evaluated in MOVAS on day 21. One representative Western Blot (K) of three independent experiments is shown. All data are presented as mean ± SEM. $*p < 0.05$, $**p < 0.01$.

This figure has been published previously in (2).

Treatment with rapamycin decreases calcification in MOVAS by promoting autophagy

To investigate the potential role of autophagy in the calcification process of MOVAS, rapamycin, a pharmacological inducer of autophagy, was used to increase autophagy in AA (50 µg/mL) and β-GP (2.5 mM) treated cells. 3-methyladenin (3-MA), a pharmacological inhibitor of autophagy, was used to decrease autophagy during the calcification process (2).

Rapamycin treatment resulted in a significant upregulation of mRNA expression of the autophagy related genes such as *Trp53in* and *Igfbp3* after 14 and 21 days (Figure 8A, B). Western Blot analysis showed that protein levels of LC3-II were 1.5-fold increased in MOVAS subjected to calcifying conditions when compared with respective controls. Treatment of MOVAS cultured under calcifying condition with rapamycin led to a threefold increase of LC3-II levels on day 21 (Figure 8C, E). Interestingly, the protein levels of p62 did not differ between MOVAS under calcifying conditions with or without rapamycin. Though, a significant decrease of p62 levels was observed in MOVAS under calcifying conditions treated with rapamycin as compared to MOVAS treated with control medium after 21 days of culture (Figure 8D, E) (2).

Next, the effect of rapamycin-induced autophagy on calcification was investigated. Despite rapamycin inducing autophagy in MOVAS only slightly, calcification of cells was decreased after treatment with rapamycin. Intensity of Alizarin Red S stained cells was attenuated on day 7 and 14 and significantly reduced after 21 days of rapamycin treatment (Figure 9A, Figure 10A). In line, measurement of cellular calcium content showed reduced calcium levels on day 7 and 14 as well as a significant decreased level of calcium after 21 days of treatment with rapamycin (Figure 9B) (2).

To explore the effect of rapamycin on the osteoblastic VSMC differentiation, *Runx2* expression was determined. qPCR revealed a significant increase of mRNA expression of *Runx2* in MOVAS cultured under calcifying conditions on day 14 and 21. Treatment with rapamycin resulted in a significant decrease of *Runx2* expression in MOVAS compared to respective controls (Figure 9E).

Additionally, gene expression of *Sm22α*, a marker for adult VSMCs, was evaluated. mRNA levels of *Sm22α* in MOVAS subjected to a calcification medium for 21 days were significantly decreased compared to MOVAS cultured with control medium. Gene expression of *Runx2* in cells under calcifying conditions treated with rapamycin was comparable with gene expression in cells subjected to control medium (Figure 9F) (2).

For a more precise characterization of the phenotype of VSMCs, α-SMA expression was analyzed using immunofluorescence staining. α-SMA is a marker for cellular contractility and was decreased in cells after 14 and 21 days of calcifying conditions. Rapamycin treatment resulted in an α-SMA expression, which was similar to the expression in cells subjected to control medium (Figure 10B) (2).

Next, the effect of inhibited autophagy on the calcification process in MOVAS was studied. For this purpose, cells under calcifying conditions were treated with 3-MA. By Western blotting we found that treatment with 3-MA for 21 days significantly decreased protein levels of LC3-II compared to cells treated with calcification medium only (Figure 8F, H). Protein levels of p62 in MOVAS treated with 3-MA under calcifying conditions were comparable with p62 levels in MOVAS cultured with control medium (Figure 8G, H) (2).

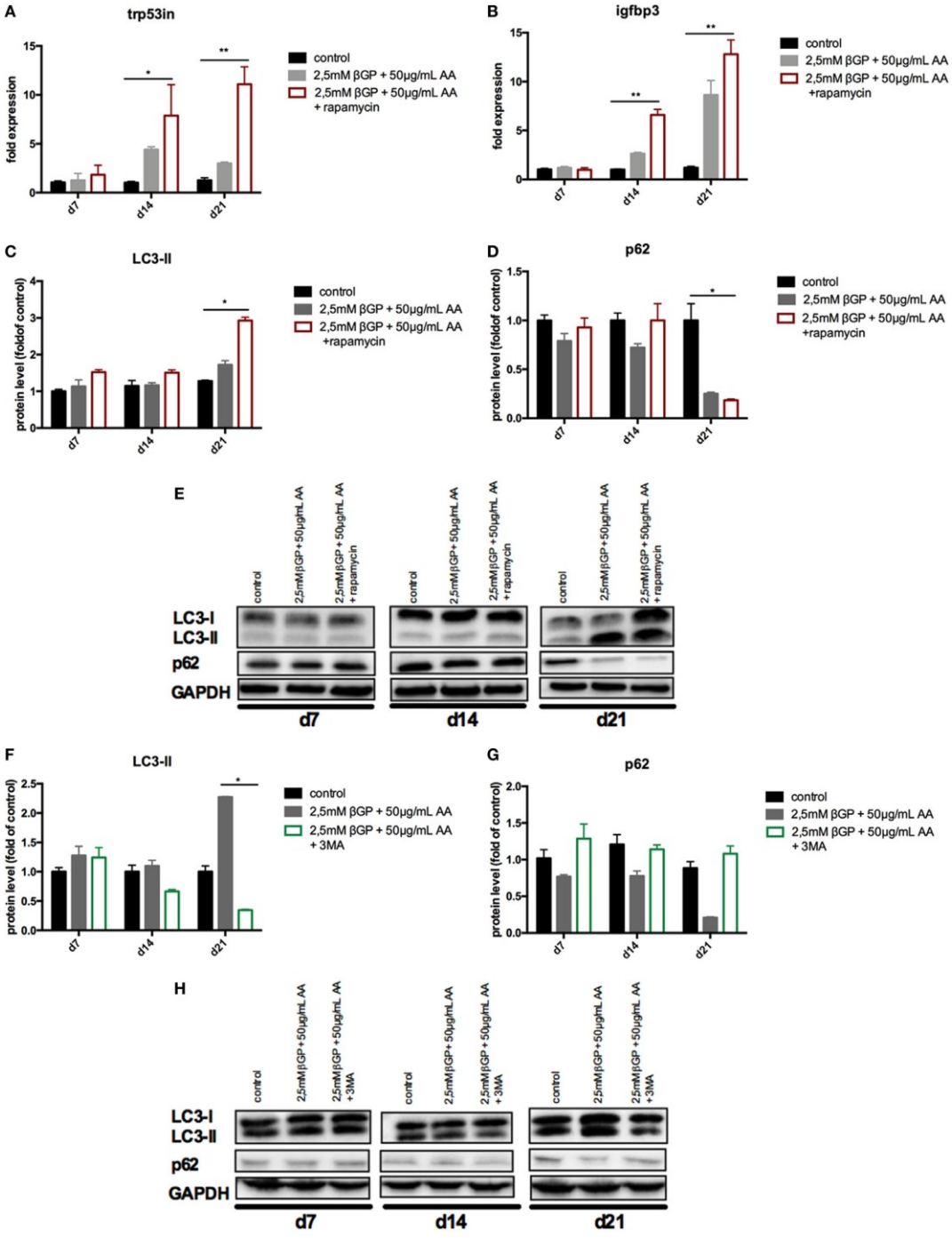

Figure 8: Treatment with Rapamycin or 3-methyladenin affects autophagy in MOVAS

MOVAS were cultured in the presence (grey bars; n=4) or absence of calcifying conditions (black bars; n=4). Additionally, cells were treated either with 10 µm rapamycin (red bars; n=4) or 5mM 3-methyladenin (green bars; n=4). qPCR analysis (A, B) of rapamycin treated cells was performed. Protein levels of LC3-II (C, F) and p62 (D, G) were detected by Western Blot (n=3). Representative Western Blots for each treatment are provided (E, H). All data are presented as mean ± SEM.

*$p < 0.05$, **$p < 0.01$. This figure has been published previously in (2).

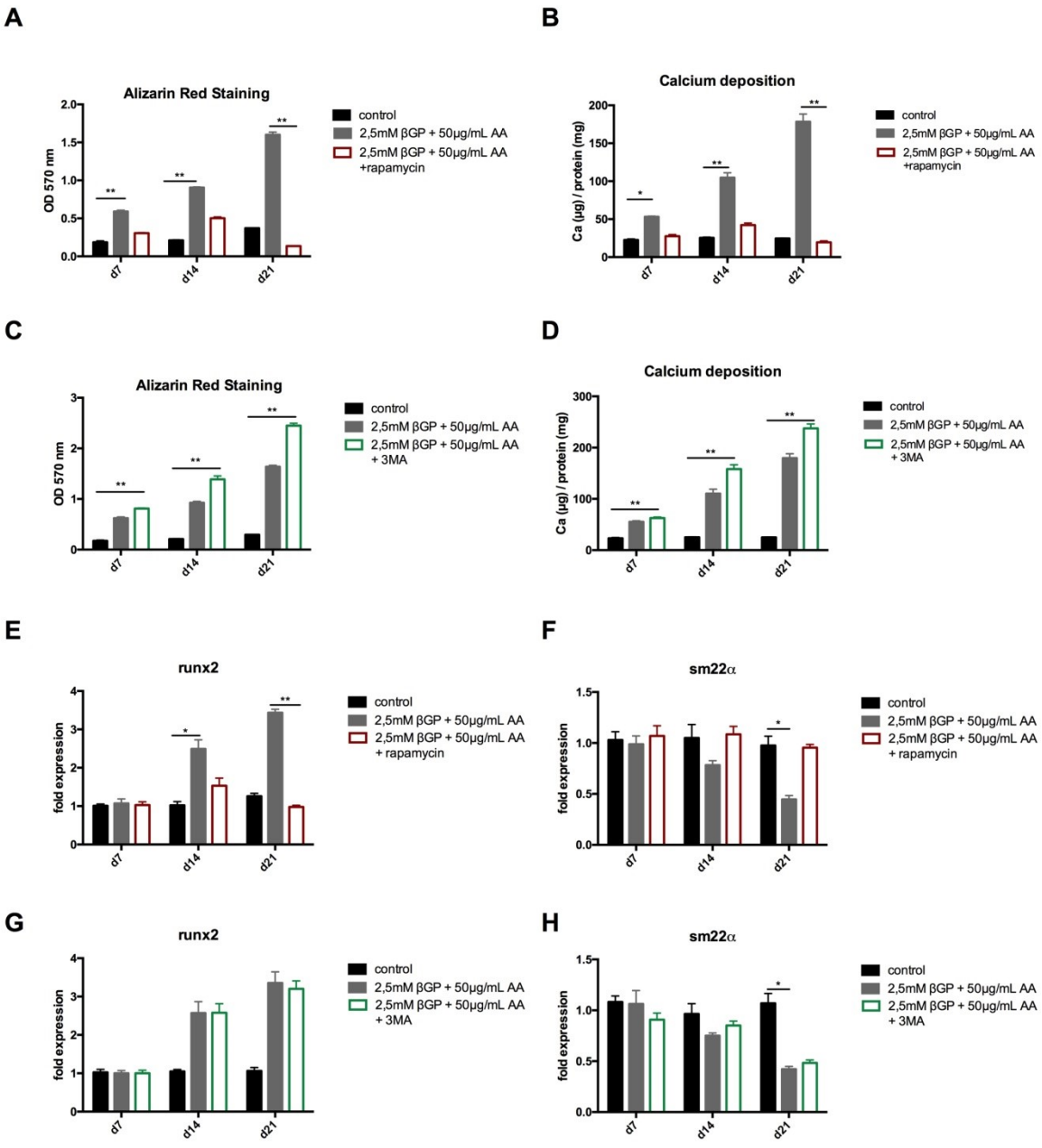

Figure 9: Modification of calcification in MOVAS by inducing or blocking autophagy

MOVAS were maintained in the presence (grey bars; n=4) or absence (black bars; n=4) of calcification medium and furthermore incubated with 10 µM rapamycin (red bars; n=4) or 5 mM 3-MA (green bars; n=4). Intensity of Alizarin Red S staining (A, C) as well as cellular calcium content (B, D) was evaluated. qPCR for *Runx2* (E, G) and *Sm22α* (F, H) was performed. All data are presented as mean ± SEM. *$p < 0.05$, **$p < 0.01$.
This figure has been published previously in (2).

To see if blocked autophagy augments calcification in VSMCs, Alizarin Red S staining as well as quantification of calcium deposition was performed. After 7, 14 and 21 days, intensity of Alizarin Red S staining was significantly increased in cells under calcifying conditions treated with 3-MA compared to cells under control conditions (Figure 9C, Figure 10A). Measurement of cellular calcium demonstrated an increase of calcification by 3-MA treatment in a time-dependent manner (Figure 9D) (2).

Real-time PCR analysis showed that mRNA levels of *Runx2* (Figure 9G) and *Sm22α* (Figure 9H) were similar in MOVAS under calcifying conditions and MOVAS under calcifying conditions treated with 3-MA. Protein expression of α-SMA was reduced in MOVAS treated with 3-MA after 14 and 21 days as compared to MOVAS under calcifying conditions (Figure 10B) (2).

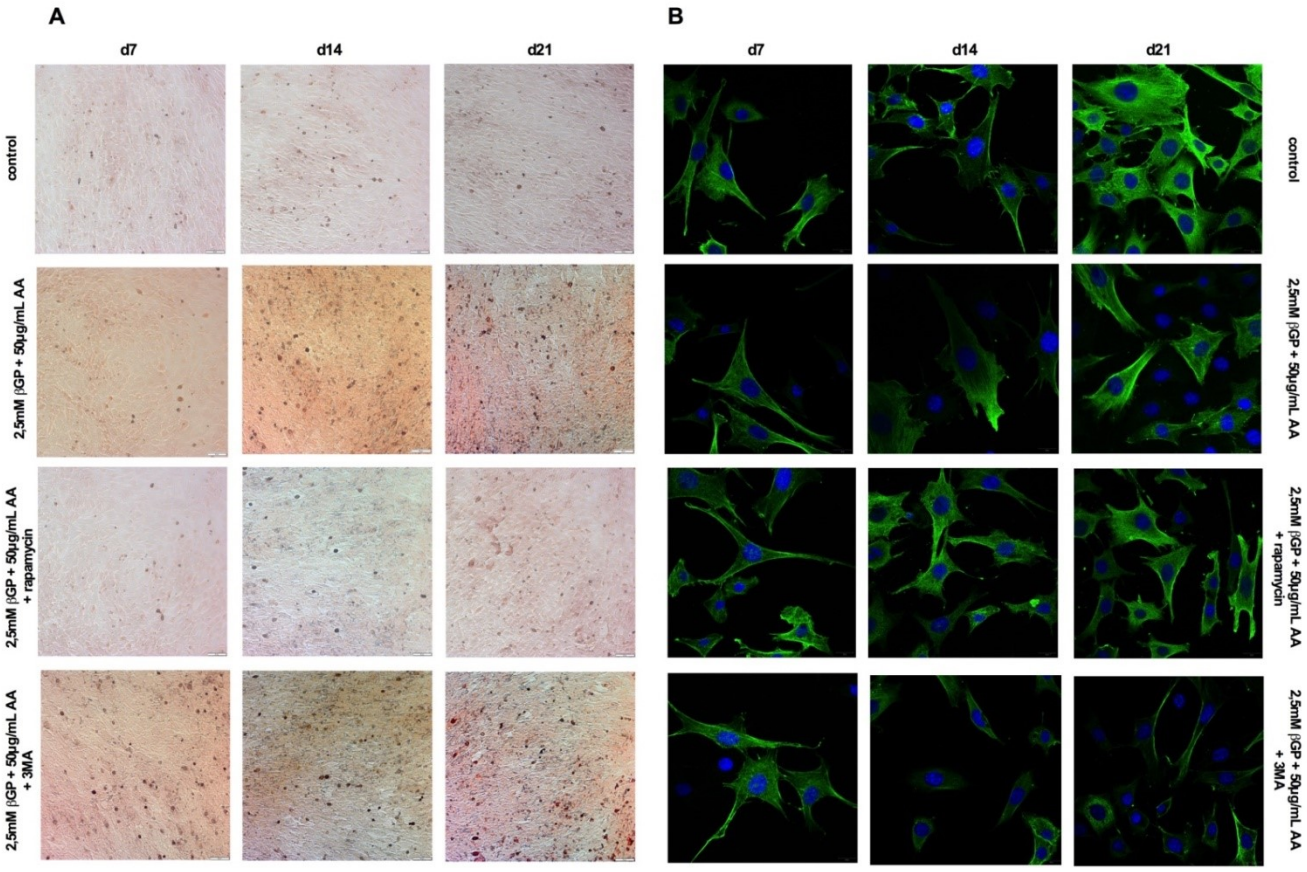

Figure 10: Calcification and α-smooth muscle actin (SMA) expression in MOVAS is affected by inducing and blocking autophagy

MOVAS were cultured in presence or absence of calcifying conditions and additionally treated with 10 µM rapamycin or to 5 mM 3-methyladenine for 7, 14, or 21 days. Representative pictures from Alizarin Red S (A) and α-SMA (B) stained cells are provided. This figure has been published previously in (2).

To confirm the results, an alternative autophagy blocker, namely Bafilomycin was used. MOVAS were cultured in presence and absence of calcifying conditions and further exposed to 20 mM bafilomycin (2). Calcification was evaluated using Alizarin Red S staining as well as determination of calcium disposition in MOVAS. Intensity of Alizarin Red S stained cells was significantly increased in MOVAS treated with bafilomycin after 7, 14 and 21 days (Figure 11A). In line, cellular calcium content was significantly augmented in bafilomycin-treated cells as compared to respective controls (Figure 11B) (2).

Gene expression of *Runx2* was significantly upregulated in MOVAS cultured under calcifying conditions when compared with MOVAS cultured with control medium, after 14 and 21 days (Figure 11C). In accordance, mRNA levels of *SM22*α were significantly reduced in cells maintained with calcification medium as compared to respective controls (Figure 11D). Gene expression of *Runx2* and *SM22*α in MOVAS cultured under calcifying conditions and additionally treated with bafilomycin was similar to gene expression of MOVAS cultured under calcifying conditions without bafilomycin treatment (Figure 11C, D) (2, 120).

After 21 days, Western Blot analysis showed a significant reduction of LC3-II protein in bafilomycin-treated MOVAS under calcifying conditions as compared to controls (Figure 11E, G). Protein levels of p62 were significantly increased in MOVAS in presence of calcification medium and additionally exposed to bafilomycin when compared with respective controls (Figure 11F, G) (2).

Thus, bafilomycin treatment in MOVAS resulted in a similar regulation pattern as rapamycin treatment (2).

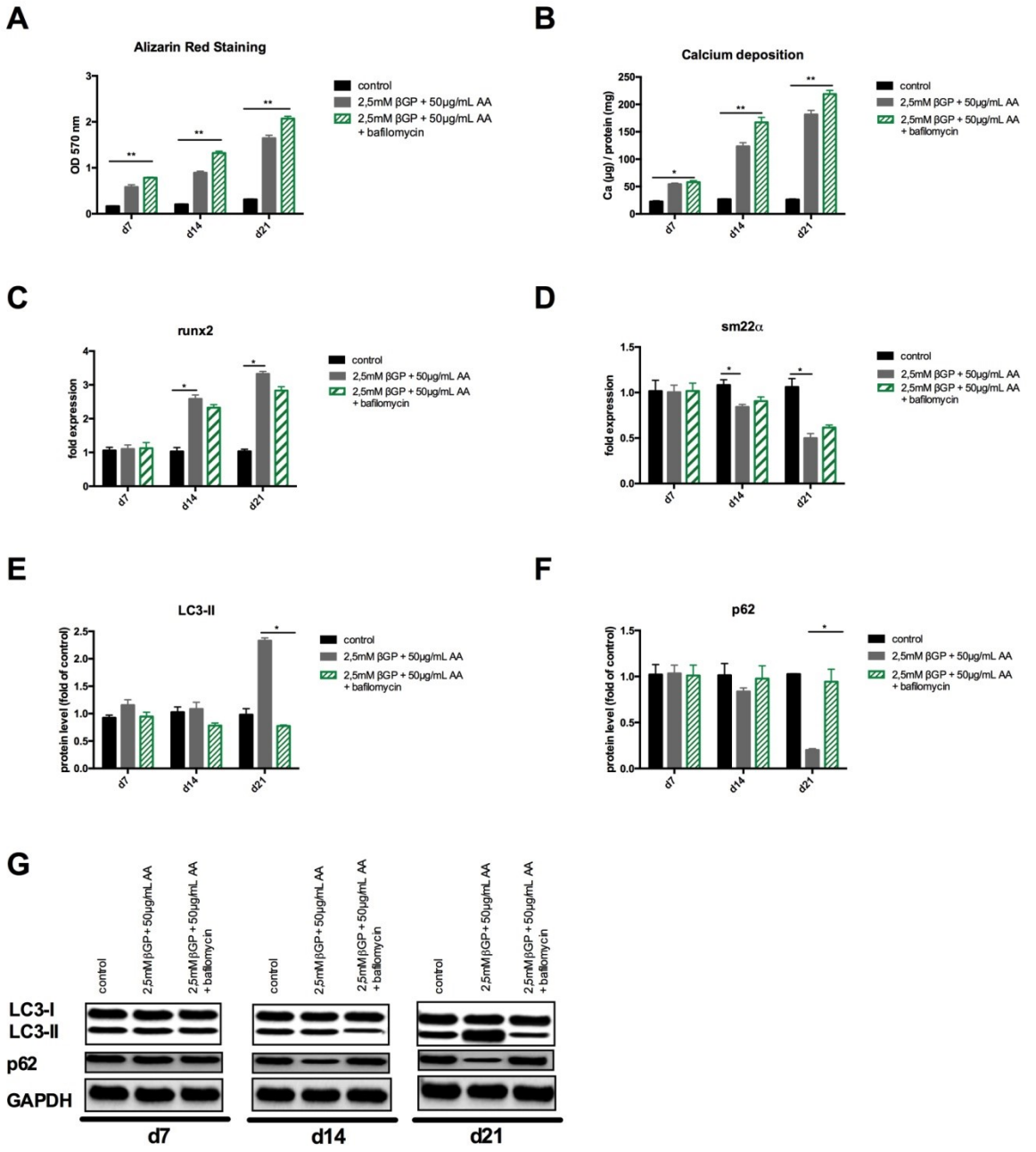

Figure 11: Treatment with Bafilomycin influences autophagy and calcification in MOVAS

MOVAS were maintained in the presence (grey bars; n=4) or absence of calcifying conditions (black bars, n=4) and additionally treated with bafilomycin (dashed green bars, n=4) for 7, 14 or 21 days. Evaluation of Alizarin Red S staining (A) as well as determination of cellular calcium content (B) was done. Gene expression of *Runx2* (C) and *Sm22α* (D) in MOVAS was analyzed using qPCR. Protein levels of LC3-II (E, G) as well as p62 (F, G) were determined by Western blotting. One representative Western Blot (G) of three independent experiments is shown. All data are presented as mean ± SEM.
$*p < 0.05$, $**p < 0.01$. This figure has been published previously in (2).

To delineate the effects of pharmacological treatment on calcification as well as the direct effect of the treatment on cells cultured with control medium, additional experiments were performed. Thus, MOVAS were maintained with control medium and exposed to rapamycin, 3-MA or bafilomycin for 7, 14 or 21 days (2).

Quantification of Alizarin Red S staining (Figure 12A) as well as measurements of calcium depositions (Figure 12B) revealed similar results between the groups. No differences in the expression of autophagy-related genes (Figure 12C-F) were detected as compared to MOVAS incubated with standard medium. The regulation pattern of LC3-II and p62 did not differ between the groups (Figure 12G-L) (2).

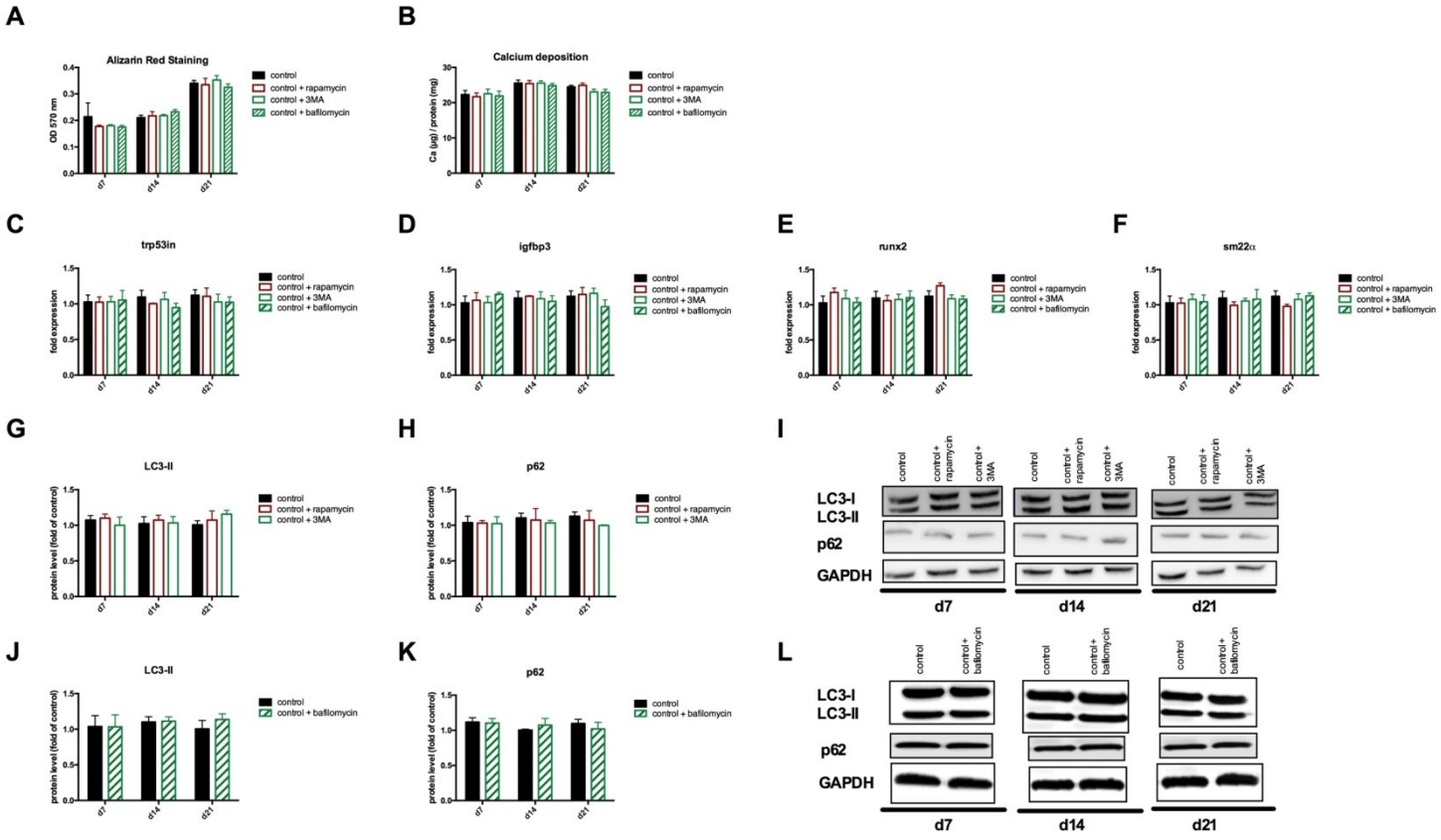

Figure 12: Calcification and Autophagy in MOVAS under non-calcifying conditions are not affected by rapamycin, 3-MA or bafilomycin treatment

MOVAS were cultured in the absence of calcifying conditions (black bars; n=4) and additionally incubated with rapamycin (red bars; n=4), 3-MA (green bars, n=4) or bafilomycin (dashed green bars; n=4) for 7, 14 or 21 days. Quantification of Alizarin Red S staining (A) as well as cellular calcium measurement (B) was performed. qPCR of autophagy-related genes (C-F) was done.

Protein levels of LC3-II (G, J) and p62 (H, K) were determined using Western Blot. One representative Western Blot (I, L) of three independent experiments is shown. All data are presented as mean ± SEM. $*p < 0.05$, $**p < 0.01$. This figure has been published previously in (2).

Treatment with rapamycin ameliorates uremic vascular media calcification in DBA/2 mice

Next, to study the role of autophagy in uremic vascular media calcification, autophagy was increased by rapamycin treatment *in vivo*. Thus DBA/2 mice were treated either with 0.5 mg rapamycin per kg body weight or with vehicle. Treatment was started 3 days before mice were set on HPD. DBA/2 mice of control groups were treated with rapamycin or vehicle and received SCD (2).

First, the renal phenotype of DBA/2 mice was explored. DBA/2 mice fed with HPD had significantly increased BUN levels (Figure 13A) as well as significantly increased renal calcium levels (Figure 13B) as compared to DBA/2 mice fed SCD. Rapamycin treatment did not change BUN or calcium levels in DBA/2 mice set on HPD (2).

Pathohistological evaluations of kidneys revealed that the glomeruli were not affected by HPD. However, HPD-fed mice developed signs of acute tubular injury mainly in the distal tubules. Distal tubular cells showed vacuolization and loss of nuclear staining as markers for beginning cell necrosis. Accordingly, treatment with rapamycin did not alter renal histology in HPD fed DBA/2 mice (Figure 13C) (2).

Real-time PCR to detect gene expression of *Trp53in*, *Igfbp3*, *Hmox1* and *Atg16l1* was performed (Figure 13D-G). The mRNA levels of these autophagy associated genes were similar between the four groups. Protein levels of LC3-II and p62 in kidneys were determined using Western Blot (Figure 13H-J). Western Blot analysis revealed that the protein levels did not differ between the four groups (2).
These findings indicate, that autophagy in kidney was not influenced by either HPD or rapamycin treatment (2).

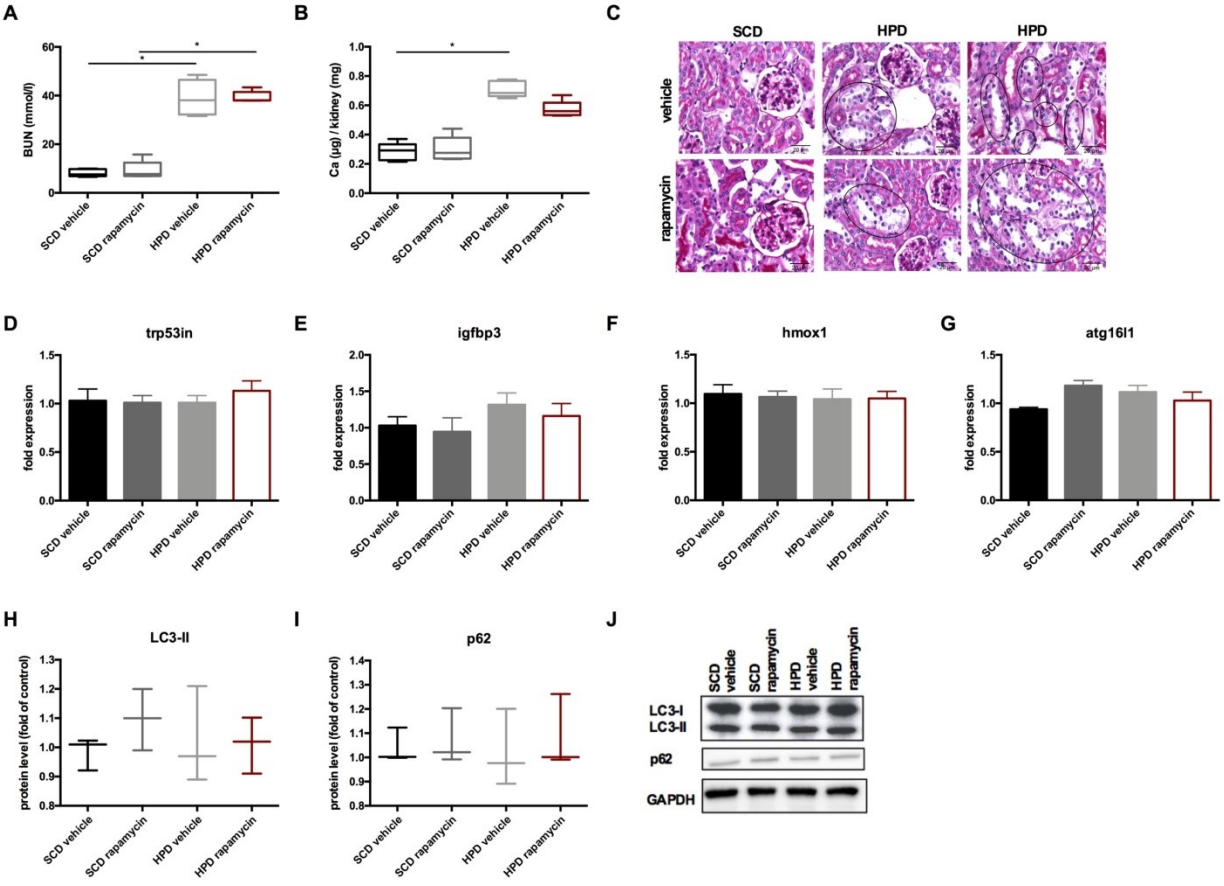

Figure 13: Renal phenotype is not influenced by rapamycin treatment

DBA/2 mice were set on high phosphate diet (HPD) or standard chow diet (SCD) for 12 days and were furthermore treated with rapamycin or vehicle from day -3. (SCD + vehicle: black bars; SCD + rapamycin: grey bars; HPD + vehicle: light grey bars; HPD + rapamycin: red bars; n=4 per group). Blood urea nitrogen (BUN) levels (A) as well as calcium content of kidneys (B) were quantitatively determined. Representative pictures of periodic acid Schiff's (PAS) stained kidney sections are shown (C). Areas of early necrotic tubular epithelial cells are marked with black circles. Real-time PCR for autophagy-related genes from renal tissue was done (D-G). Western Blot analysis to detect protein levels of LC3-II and p62 in kidneys was done. Three independent experiments were performed. A representative Western Blot is provided (J). $*p < 0.05$.

This figure has been published previously in (2).

In order to explore the vascular phenotype in DBA/2 mice, aortas were isolated and evaluated.

First, expression of autophagy related genes was determined using qPCR (Figure 14A). mRNA levels of *Trp53in*, *Igfbp3*, *Hmox1*, *Adrb2* and *Atg16l1* were significantly increased in DBA/2 mice fed HPD and treated with rapamycin. In line, a significant increase of LC3-II protein levels and a significant decrease of p62 protein levels was observed in rapamycin-treated mice set on HPD when compared with respective controls (Figure 14C-E) (2).

Interestingly, rapamycin treatment inverted the increase of pro-inflammatory cytokine mRNA expression such as *Tnf-alpha* and *Il6* in aortic tissue of mice fed HPD. In accordance, *Tbx21*, the master regulator for TH1 differentiation in mice, was downregulated by rapamycin treatment in DBA/2 mice fed HPD. Gene expression of *Foxp3*, the master gene regulator of regulatory T cells, was significantly upregulated by rapamycin treatment in aortas of HPD mice (Figure 14B) (2).

Next, the influence of rapamycin treatment on vascular calcification was investigated. Determination of aortic calcification by measuring the calcium content of aortas revealed a significant reduction of calcium in rapamycin treated HPD mice when compared with vehicle treated HPD mice (Figure 14F). mRNA levels of *Runx2* were significantly downregulated in aortas of mice fed HPD and treated with rapamycin as compared to vehicle HPD mice. Of note, after rapamycin treatment, calcium levels as well as gene expression levels of *Runx2* of HPD mice were decreased to the levels that were found in aortas of SCD mice (Figure 14G) (2).

Previous data showed, that DBA/2 mice fed with HPD die because of remarkable cardiovascular calcification, which leads to bradycardia and sudden cardiac death (110). This finding was the reason why we wanted to know if rapamycin-treatment had an impact on survival rate in DBA/2 mice fed HPD. DBA/2 mice set on HPD and treated with rapamycin survived significantly longer as compared to HPD mice treated with vehicle (Figure 14H) (2).

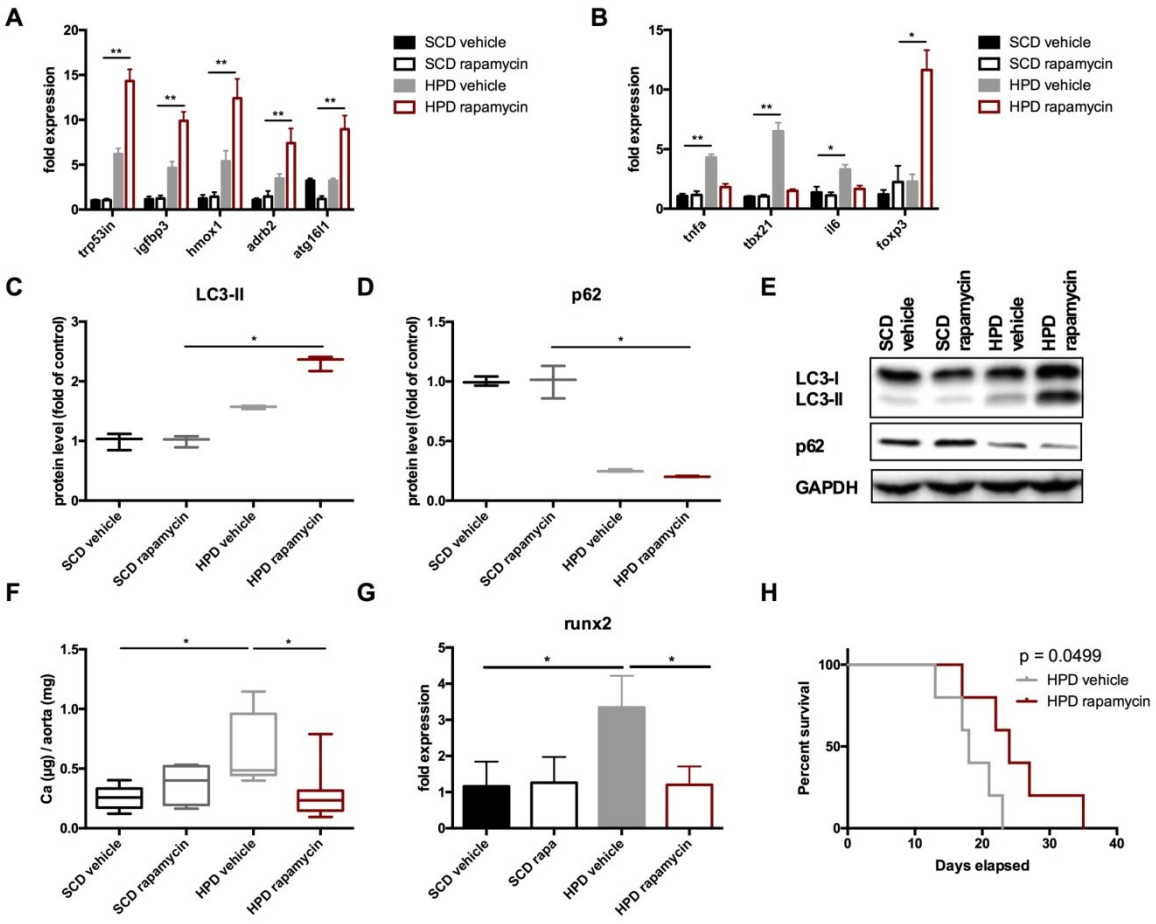

Figure 14: Rapamycin-induced autophagy improves uremic vascular media calcification

DBA/2 mice were fed with high-phosphate diet (HPD) or standard chow diet (SCD) for 12 days and were additionally treated with rapamycin or vehicle from day -3. (SCD + vehicle: black bars; SCD + rapamycin: grey bars; HPD + vehicle: light grey bars; HPD + rapamycin: red bars; n=4 per group). qPCR analysis to evaluate autophagy associated genes (A) as well as inflammatory genes (B) in aortas was done. Protein levels of LC3-II (C) and p62 (D) were determined using Western Blot analysis. Three independent experiments were performed. A representative Western Blot (E) is provided. Quantification of total calcium content (F) in aortic tissue was done. Expression of *Runx2* (G) in aortas was evaluated by performing qPCR. A Kaplan-Meier plot of mice set on HPD and treated with either vehicle (grey line) or Rapamycin (red line) is shown (H; n=14 per group). All data are presented as mean ± SEM. *$p < 0.05$, **$p < 0.01$.

This figure has been published previously in (2).

Treatment with rapamycin delays progression of established uremic vascular media calcification in DBA/2 mice

To provide evidence for the suitability of rapamycin for therapeutic treatment, the efficiency of rapamycin to ameliorate already established uremic vascular media calcification was evaluated. For this purpose, rapamycin treatment was started on day 5 of high-phosphate treatment and followed until day 12 (2).

In order to test if later started rapamycin treatment would still results in increased autophagy, protein levels of LC3-II and p62 were detected by Western Blotting. Protein expression of LC3-II (Figure 15A, C) as wells as p62 levels (Figure 15B, C) was not significantly influenced by rapamycin treatment in DBA/2 mice fed HPD (2).
However, total calcium content of aortas was significantly reduced in rapamycin-treated mice set on HPD when compared with vehicle treated HPD mice (Figure 15D) (2).

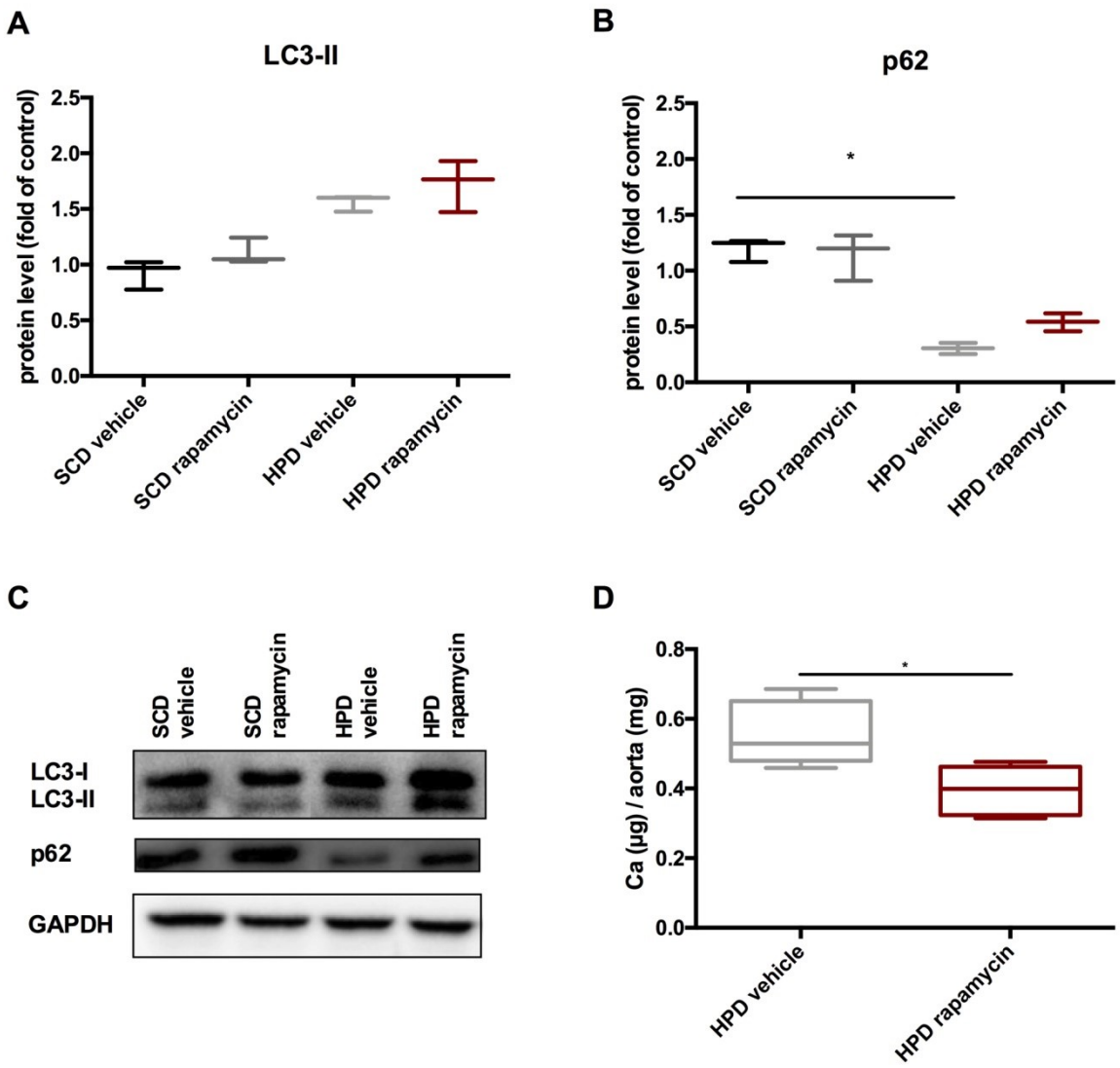

Figure 15: Rapamycin treatment ameliorates uremic vascular calcification in DBA/2 mice with present vascular calcification.

DBA/2 mice were fed with high-phosphate diet (HPD) or standard chow diet (SCD) for 12 days and additionally treated with rapamycin or vehicle from day 5. (SCD + vehicle: black bars; SCD + rapamycin: grey bars; HPD + vehicle: light grey bars; HPD + rapamycin: red bars). Protein levels of LC3-II (A) as well as p62 (B) were detected using Western Blot analysis (n=3). A representative Western Blot is provided (C). Quantification of total calcium content of aortic tissue (D) was done (n=5). All data are presented as mean ± SEM. *$p < 0.05$.

This figure has been published previously in (2).

Discussion

In the last decades CKD became a global health problem, affecting approximately 10% of adults worldwide (5). clinical The definition, diagnosis, and evaluation of CKD, including CKD-MBD were important milestones in recent clinical nephrology (75, 122). Current research is focused on the pathogenesis of CKD and its various deleterious complications (122, 123). The need for a deeper understanding of CKD derives from the fact that patients suffering from CKD stage 4-5 are ultimately dependent on renal replacement therapy which is associated with increased mortality, morbidity and reduced quality of life.
In order to address these research needs, different animal models have been developed. For the present doctoral thesis, we used DBA/2 mice on high-phosphate diet. In the first part of this thesis we put a strong emphasis on the impact of CKD on mineral bone disorder. In the second part of the thesis, we focused on the impact of CKD on vascular media calcification

Taken together, the findings of part A of the thesis allow postulating a new model of chronic kidney diseases. This murine model of CKD reflects important features of mineral and bone disorder, such as vascular media calcification, secondary hyperparathyroidism, and low-turnover bone disease (1).

The conventional model to investigate chronic kidney disease is the 5/6 nephrectomy model. The disadvantage of this model is that it is problematic to induce robust CKD in mice and it that is also challenging to reproduce surgery conditions leading to the same outcomes. For this reason, many researchers are working with the CKD model established by *Gagnon et al*. In this model, chronic kidney disease is induced by coagulating the renal surface of one kidney and after some weeks of recovery a nephrectomy of the other kidney is performed (124). Still, the rate of mortality during and after this invasive intervention is very high and the surgical procedure, which is essential to induce chronic kidney diseases, causes a lot of bias (84, 124).
In contrast, our model is not based on surgical interventions which results in a low mortality rate (5 to 10%), since we stop the high-phosphate treatment on day 4 or 7, respectively (1). As recently published, the survival of DBA/2 mice significantly decreases when mice are set on high-phosphate diet for more than 10 days (110). Due to the fact that

C57BL/6 mice do not develop remarkable renal calcification or any calcification of the cardiovascular system, it is very important to use DBA/2 mice for our CKD-MBD model (125). DBA/2 mice are prone to developing tissue calcification, because this mouse strain has an alternative splice variant of the *Abcc6* gene (86, 88).

In our murine CKD-MBD model, DBA/2 mice develop chronic kidney disease according to the human equivalent of stage 3 in CKD. This is shown by a 50% reduction of glomerular filtration rate in HPD mice when compared to control mice (1). On the contrary, mice with surgically induced chronic kidney disease normally correspond to a CKD stage 5 in humans (84, 126, 127).

Therefore, our murine model is suitable to investigate changes and alterations in various organs in early stages of CKD-MBD. This opportunity is of high importance because only early started therapeutic interventions seem to be successful in improving mortality and morbidity in patients suffering from CKD.

The results of our studies revealed that CKD mice develop cardiovascular changes such as media sclerosis in the abdominal aorta. Since we had a low number of mice for echocardiographic evaluations and the heart weights were similar between the groups, it is hardly possible to determine if the CKD mice additionally developed concentric left ventricular hypertrophy (1). Previously data showed that mice with HPD-induced acute kidney injury suffer from a dystrophic cardiac calcinosis, which leads to a significantly increased mortality rate in these mice (110). In contrast, the here presented CKD-MBD model displayed a different cardiac phenotype, since HPD fed mice did not develop calcifications in the myocardium. Nevertheless, preliminary observation using echocardiography revealed that CKD mice developed some extent of cardiac hypertrophy (1). One explanation for this observation could be that the mice might have hypertension, which would reflect the human equivalent of CKD-MBD (1). To extensively describe the cardiovascular changes as well as the cardiac phenotype, additionally evaluations such as blood pressure measurement and an increase of n-numbers in echocardiographic analysis are indispensable.

In our murine CKD-MBD model, media sclerosis was mainly located in the abdominal aorta, which was consistent with previous data from our group published in a high-phosphate induced uremic calcification mouse model (1, 111). *Kirsch et al.* showed that in patients with CKD as well as in DBA/2 mice with CKD, the abdominal aorta was more

prone to vascular media calcification as compared to the ascending aorta (111). The underlying mechanism to explain this finding is still under investigation. A possible explanation could be the different developmental origins of vascular smooth muscle cells, which results in a different susceptibility to calcify according to the different parts of the aorta (111, 128).

The DBA/2 mice in our CKD-MBD model displayed a low-turnover bone disease, which was determined by bone histomorphometric evaluations, although serum parathyroid hormone levels were significantly increased in mice with chronic kidney disease (1). This shows that Pth is not a suitable biomarker to diagnose bone disease in CKD. Instead bone histomorphometry should be used for analyzing and detecting of bone disease in CKD (24, 75).
Measurements of serum Fgf-23 revealed a significant increase in HPD-fed mice when compared to SCD fed mice after 14 days. Interestingly, on day 84 no difference in Fgf-23 levels between the groups was detectable (1). Apparently, the early Fgf-23 increase is a physiological reaction to compensate the oral high-phosphate intake. Since mice were subsequently set on SCD after HDP treatment, Fgf-23 levels normalize within the following days. Recently, *Graciolli et al.* described an increased expression of Ffg-23 in patients with renal osteodystrophy (129). Thus, it would be interesting to investigate the role of Ffg-23 in the bone of DBA/2 mice in our CKD-MBD in detail.

The present murine model is the first experimental CKD model which is accompanied by a low-turnover bone disorder (1). Another existing CKD model is surgically induced by subtotal nephrectomy and describes renal osteodystrophy (84, 126, 127). In contrast to our CKD-MBD model, histomorphometrical analysis was done in the lumbar vertebrae (84). *Cejka et al.* also performed microCT evaluations in the tibia-trabecular area and their mice displayed increased bone volume and decreased bone mineralization (84). However, the mice in our CKD-MBD model revealed decreased bone volume as well as decreased mineralization in the tibia (1). Further analysis of the bone phenotype in our CKD-MBD is still necessary. For example, histological evaluation as well as confocal microscopy of the bone could be performed to explore the murine model in detail.
Nevertheless, we present a model of chronic kidney disease which reflects important features of the human equivalent and represents a useful tool for the investigation of pathogenic features of the mineral and bone metabolism in CKD as well as treatment options of CKD-MBD without the need for surgical methods (1).

The research question of part B of the present thesis was focused on the investigation of the role of autophagy in the uremic media calcification.

Our findings represent convincing evidence that uremic media calcification results in an increased autophagy in vascular smooth muscle cells both *in vitro* and *in vivo.* The autophagic process is an endogenous and protective response to vascular calcification, whereas autophagy increased by pharmacological treatment even improves uremic media calcification (2).

Existing murine models have already showed that autophagy is a protective mechanism to counteract atherosclerosis, but those models mostly use Apo E knockout mice. This mouse strain is optimal to mimic human atherosclerosis, contrary our model with DBA/2 mice, which reflects uremic media calcification (2, 111, 112, 120). Uremic media calcification and atherosclerosis are different in their histological phenotype as well as in their underlying pathomechanisms (73). The data on the role of autophagy in uremic media calcification are rare, only *Dai et al*. showed that stimulation of vascular smooth muscle cells under high-phosphate conditions results in protections from calcification due to increased autophagy in cells (118). First of all, we could confirm the *in vitro* findings published from *Dai et al*. and furthermore we were able to extend the finding to the *in vivo* situation (2, 118, 120).

For our studies we used a murine model of uremia induced by treatment with HPD and additionally characterized by remarkable vascular media calcification (111). We showed that the calcification of the *tunica media* comes along with an increase of autophagy in VSMCs. Rapamycin treatment started on day -3 in DBA/2 mice fed HPD leads to an increase of autophagy resulting in a reduction of aortic calcification as well as in an extension of the life span of DBA/2 mice. Furthermore, rapamycin treatment was also efficiently decreased calcification in aortas when mice already had established vascular calcification (2).

To prove that the decreased vascular calcification is not a side effect of improved kidney function by rapamycin treatment, the kidney phenotype was evaluated. We found that the protective effects of treatment with rapamycin were not affecting kidney function, since neither renal function nor calcification was changed by rapamycin (2). Up to now, we can only hypothesize about the different susceptibility to protection from calcification by autophagy induction in aortas and kidneys. One explanation could be that the calcification

process in the kidney is characterized by a higher severity compared to aortic calcification, which is why the body reacts in form of a necrosis instead of inducing autophagy (2).
A major limitation of our experimental setup in DBA/2 mice is the fact that rapamycin is accompanied by systemic anti-inflammatory effects. We cannot totally exclude that the improved outcome of rapamycin-treated mice is caused by the systemic anti-inflammatory effects of the treatment per se (2).
Rapamycin is an immunosuppressive compound produced by *Streptomyces hygroscopicus* and can be used to induce proliferation of regulatory T cells *in vitro* and *in vivo (130, 131).* Accordingly, transcription levels of *Foxp3* were significantly increased in aortas of rapamycin-treated mice as compared to vehicle-treated mice, whereas the expression of the regulator of TH1 differentiation as well as the expression of macrophage marker were supressed (2). Nevertheless, the precise role of inflammation in the pathogenesis of uremic vascular media calcification is still unclear (73, 111, 132). Previous data from our group showed that infiltration of immune cells in aortas of DBA/2 mice suffering from uremic media calcification is a secondary phenomenon induced by vascular calcification (111). Hence, *in vivo* experiments using autophagy inducers which are more specific and do not affect the immune system, such as TAT-Beclin (133), are needed to investigate the impact of autophagy on media vascular calcification as well as on the survival rate of mice (2).

Another method to induce autophagy in cells is fasting, in form of a nutrient and amino acid deficiency. This mechanism could also play a role for the *in vivo* model, since DBA/2 mice on HPD reduce food intake resulting in a significant drop of body weight (2).
Besides, autophagy can be induced by the production of ROS. *Dai et al.* provided evidence that this activation pathway is involved in phosphate-induced autophagy in VSMCs (118). In our murine model we detected signs of elevated ROS production in aortas of HPD-fed mice, which were evaluated using the NBT staining technique (2). Nevertheless, to describe the role of ROS production in our *in vivo* model in detail, additional experiments are necessary.
Furthermore, there are recent data suggesting that inflammasomes and autophagy regulate each other. On the one hand an autophagic process results in removal of intracellular DAMPs, inflammasome components, or cytokines, which leads to a reduction of inflammasome activation. On the other hand, inflammasome activation can increase autophagy to protect from excessive inflammation (134-137). Previous data demonstrated that the autophagy related gene *Agt16l1* is a fundamental component in the process of

autophagy to control of the endotoxin-induced inflammatory immune response and is therefore linked with inflammasome. Thus, depletion of *Atg16l1* results in an increased endotoxin-induced IL-1 beta production (138). We detected a significant increase of the gene expression of *Atg16l1* in aortas of mice treated with HPD, but we do not find alterations in transcription levels of *Il-1beta* in aortic samples of HPD fed mice. This leads to the assumption that this pathway plays no role in the calcification process of the aorta in our uremic model (2).

Most of the pathways to activate autophagic processes are linked with the mTOR-pathway, but also some independent pathways have been described (112). While autophagy is a cell survival mechanism, it can also promote cell death if the cellular damage becomes irreparable (139). Therefore, it has been suggested that autophagy reduces the matrix vesicle release in VSMCs, since the formation of matrix vesicle is essential for the calcification process (118). But further investigation is needed to prove if the formation and the release of matrix vesicle is also crucial in the *in vivo* situation.
In contrast to *Dai et al.* we found that mRNA levels of *Runx2*, a marker of osteogenic transdifferentiation of VSMCs *(140)*, were significantly increased under calcifying conditions both *in vivo* and *in vitro* (2). Of note, rapamycin treatment resulted in significantly decreased transcription levels of *Runx2* in MOVAS under calcifying conditions as well as in aortas of DBA/2 mice fed HPD (2). According to our hypothesis, that autophagy inhibits osteogenic trans-differentiation of VSMCs, gene expression of *SM22α* and protein expression of α-SMA were both increased in MOVAS treated with rapamycin, while MOVAS treated with 3-MA displayed decreased expression of α-SMA as well as of *SM22α* (2). Osteogenic transdifferentiation of VSMCs is associated with reduced expression of both α-SMA and SM22α (141) (142).

To conclude, autophagy is an endogenous protective response of VSMC during uremia to protect from calcification by probably by inhibiting osteogenic transdifferentiation of VSMCs. This leads to the assumption that increasing autophagy could be an attractive treatment strategy to improve vascular calcification in patients suffering from CKD and ESRD (2, 120).

CKD is characterized by a disturbed mineral and bone metabolism and also associated with a high risk of vascular calcification (13). These severe complications of CKD were subject of the present thesis that investigated the bone-kidney axis in CKD using a novel animal model. In part A, we established a murine model of CKD which may serve as useful tool to test potential therapeutic interventions in CKD-MBD. In part B we took a step forward, focused on the cardiovascular endpoints, and clearly demonstrate that autophagy protects from uremic media calcification in our animal model. Thus, these investigations might pave the way towards new pharmacological principles for the treatment of CKD and its deleterious clinical complications.

Bibliography

1. Frauscher B, Artinger K, Kirsch AH, Aringer I, Moschovaki-Filippidou F, Ketszeri M, et al. A New Murine Model of Chronic Kidney Disease-Mineral and Bone Disorder. Int J Endocrinol. 2017;2017:1659071.

2. Frauscher B, Kirsch AH, Schabhuttl C, Schweighofer K, Ketszeri M, Pollheimer M, et al. Autophagy Protects From Uremic Vascular Media Calcification. Front Immunol. 2018;9:1866.

3. Levin A, Stevens PE. Summary of KDIGO 2012 CKD Guideline: behind the scenes, need for guidance, and a framework for moving forward. Kidney Int. 2014;85(1):49-61.

4. Makris K, Spanou L. Acute Kidney Injury: Definition, Pathophysiology and Clinical Phenotypes. Clin Biochem Rev. 2016;37(2):85-98.

5. Hill NR, Fatoba ST, Oke JL, Hirst JA, O'Callaghan CA, Lasserson DS, et al. Global Prevalence of Chronic Kidney Disease - A Systematic Review and Meta-Analysis. PLoS One. 2016;11(7):e0158765.

6. Bruck K, Stel VS, Gambaro G, Hallan S, Volzke H, Arnlov J, et al. CKD Prevalence Varies across the European General Population. J Am Soc Nephrol. 2016;27(7):2135-47.

7. Cerda J, Lameire N, Eggers P, Pannu N, Uchino S, Wang H, et al. Epidemiology of acute kidney injury. Clin J Am Soc Nephrol. 2008;3(3):881-6.

8. Ali T, Khan I, Simpson W, Prescott G, Townend J, Smith W, et al. Incidence and outcomes in acute kidney injury: a comprehensive population-based study. J Am Soc Nephrol. 2007;18(4):1292-8.

9. Levey AS, Stevens LA, Coresh J. Conceptual model of CKD: applications and implications. Am J Kidney Dis. 2009;53(3 Suppl 3):S4-16.

10. Levey AS, Eckardt KU, Tsukamoto Y, Levin A, Coresh J, Rossert J, et al. Definition and classification of chronic kidney disease: a position statement from Kidney Disease: Improving Global Outcomes (KDIGO). Kidney Int. 2005;67(6):2089-100.

11. Stevens PE, Levin A, Kidney Disease: Improving Global Outcomes Chronic Kidney Disease Guideline Development Work Group M. Evaluation and management of chronic kidney disease: synopsis of the kidney disease: improving global outcomes 2012 clinical practice guideline. Ann Intern Med. 2013;158(11):825-30.

12. Abutaleb N. Why we should sub-divide CKD stage 3 into early (3a) and late (3b) components. Nephrol Dial Transplant. 2007;22(9):2728-9.

13. Go AS, Chertow GM, Fan D, McCulloch CE, Hsu CY. Chronic kidney disease and the risks of death, cardiovascular events, and hospitalization. N Engl J Med. 2004;351(13):1296-305.

14. Kazancioglu R. Risk factors for chronic kidney disease: an update. Kidney Int Suppl (2011). 2013;3(4):368-71.

15. Lea JP, Nicholas SB. Diabetes mellitus and hypertension: key risk factors for kidney disease. J Natl Med Assoc. 2002;94(8 Suppl):7S-15S.

16. McClellan WM, Flanders WD. Risk factors for progressive chronic kidney disease. J Am Soc Nephrol. 2003;14(7 Suppl 2):S65-70.

17. Bruno G, Merletti F, Bargero G, Novelli G, Melis D, Soddu A, et al. Estimated glomerular filtration rate, albuminuria and mortality in type 2 diabetes: the Casale Monferrato study. Diabetologia. 2007;50(5):941-8.

18. Tozawa M, Iseki K, Iseki C, Kinjo K, Ikemiya Y, Takishita S. Blood pressure predicts risk of developing end-stage renal disease in men and women. Hypertension. 2003;41(6):1341-5.

19. Ravera M, Re M, Deferrari L, Vettoretti S, Deferrari G. Importance of blood pressure control in chronic kidney disease. J Am Soc Nephrol. 2006;17(4 Suppl 2):S98-103.

20. Chang A, Kramer H. CKD progression: a risky business. Nephrol Dial Transplant. 2012;27(7):2607-9.

21. Ejerblad E, Fored CM, Lindblad P, Fryzek J, McLaughlin JK, Nyren O. Obesity and risk for chronic renal failure. J Am Soc Nephrol. 2006;17(6):1695-702.

22. Vikse BE, Irgens LM, Leivestad T, Hallan S, Iversen BM. Low birth weight increases risk for end-stage renal disease. J Am Soc Nephrol. 2008;19(1):151-7.

23. Luyckx VA, Brenner BM. The clinical importance of nephron mass. J Am Soc Nephrol. 2010;21(6):898-910.

24. Moe S, Drueke T, Cunningham J, Goodman W, Martin K, Olgaard K, et al. Definition, evaluation, and classification of renal osteodystrophy: a position statement from Kidney Disease: Improving Global Outcomes (KDIGO). Kidney Int. 2006;69(11):1945-53.

25. Nigwekar SU, Tamez H, Thadhani RI. Vitamin D and chronic kidney disease-mineral bone disease (CKD-MBD). Bonekey Rep. 2014;3:498.

26. Mejia N, Roman-Garcia P, Miar AB, Tavira B, Cannata-Andia JB. Chronic kidney disease--mineral and bone disorder: a complex scenario. Nefrologia. 2011;31(5):514-9.

27. Cunningham J, Locatelli F, Rodriguez M. Secondary hyperparathyroidism: pathogenesis, disease progression, and therapeutic options. Clin J Am Soc Nephrol. 2011;6(4):913-21.

28. Berndt TJ, Schiavi S, Kumar R. "Phosphatonins" and the regulation of phosphorus homeostasis. Am J Physiol Renal Physiol. 2005;289(6):F1170-82.

29. Penido M, Alon US. Phosphate homeostasis and its role in bone health. Pediatr Nephrol. 2012;27(11):2039-48.

30. Farrow EG, White KE. Recent advances in renal phosphate handling. Nat Rev Nephrol. 2010;6(4):207-17.

31. Prie D, Urena Torres P, Friedlander G. Latest findings in phosphate homeostasis. Kidney Int. 2009;75(9):882-9.

32. Isakova T, Wahl P, Vargas GS, Gutierrez OM, Scialla J, Xie H, et al. Fibroblast growth factor 23 is elevated before parathyroid hormone and phosphate in chronic kidney disease. Kidney Int. 2011;79(12):1370-8.

33. Isakova T, Wolf MS. FGF23 or PTH: which comes first in CKD ? Kidney Int. 2010;78(10):947-9.

34. Hill KM, Martin BR, Wastney ME, McCabe GP, Moe SM, Weaver CM, et al. Oral calcium carbonate affects calcium but not phosphorus balance in stage 3-4 chronic kidney disease. Kidney Int. 2013;83(5):959-66.

35. Olauson H, Lindberg K, Amin R, Jia T, Wernerson A, Andersson G, et al. Targeted deletion of Klotho in kidney distal tubule disrupts mineral metabolism. J Am Soc Nephrol. 2012;23(10):1641-51.

36. Brandenburg VM, Floege J. Adynamic bone disease-bone and beyond. NDT Plus. 2008;1(3):135-47.

37. Jamal SA, West SL, Miller PD. Fracture risk assessment in patients with chronic kidney disease. Osteoporos Int. 2012;23(4):1191-8.

38. Alem AM, Sherrard DJ, Gillen DL, Weiss NS, Beresford SA, Heckbert SR, et al. Increased risk of hip fracture among patients with end-stage renal disease. Kidney Int. 2000;58(1):396-9.

39. Ott SM. Histomorphometric measurements of bone turnover, mineralization, and volume. Clin J Am Soc Nephrol. 2008;3 Suppl 3:S151-6.

40. Dempster DW, Compston JE, Drezner MK, Glorieux FH, Kanis JA, Malluche H, et al. Standardized nomenclature, symbols, and units for bone histomorphometry: a 2012 update of the report of the ASBMR Histomorphometry Nomenclature Committee. J Bone Miner Res. 2013;28(1):2-17.

41. Sherrard DJ, Hercz G, Pei Y, Maloney NA, Greenwood C, Manuel A, et al. The spectrum of bone disease in end-stage renal failure--an evolving disorder. Kidney Int. 1993;43(2):436-42.

42. Salmon B, Bardet C, Coyac BR, Baroukh B, Naji J, Rowe PS, et al. Abnormal osteopontin and matrix extracellular phosphoglycoprotein localization, and odontoblast differentiation, in X-linked hypophosphatemic teeth. Connect Tissue Res. 2014;55 Suppl 1:79-82.

43. London G, Coyne D, Hruska K, Malluche HH, Martin KJ. The new kidney disease: improving global outcomes (KDIGO) guidelines - expert clinical focus on bone and vascular calcification. Clin Nephrol. 2010;74(6):423-32.

44. Jablonski KL, Chonchol M. Vascular calcification in end-stage renal disease. Hemodial Int. 2013;17 Suppl 1:S17-21.

45. Foley RN, Parfrey PS. Cardiovascular disease and mortality in ESRD. J Nephrol. 1998;11(5):239-45.

46. Giachelli CM. The emerging role of phosphate in vascular calcification. Kidney Int. 2009;75(9):890-7.

47. Verberckmoes SC, Persy V, Behets GJ, Neven E, Hufkens A, Zebger-Gong H, et al. Uremia-related vascular calcification: more than apatite deposition. Kidney Int. 2007;71(4):298-303.

48. Foley RN, Parfrey PS, Sarnak MJ. Clinical epidemiology of cardiovascular disease in chronic renal disease. Am J Kidney Dis. 1998;32(5 Suppl 3):S112-9.

49. Guerin AP, London GM, Marchais SJ, Metivier F. Arterial stiffening and vascular calcifications in end-stage renal disease. Nephrol Dial Transplant. 2000;15(7):1014-21.

50. Abedin M, Tintut Y, Demer LL. Vascular calcification: mechanisms and clinical ramifications. Arterioscler Thromb Vasc Biol. 2004;24(7):1161-70.

51. Hruska KA, Saab G, Mathew S, Lund R. Renal osteodystrophy, phosphate homeostasis, and vascular calcification. Semin Dial. 2007;20(4):309-15.

52. Shroff R, Long DA, Shanahan C. Mechanistic insights into vascular calcification in CKD. J Am Soc Nephrol. 2013;24(2):179-89.

53. Kendrick J, Chonchol M. The role of phosphorus in the development and progression of vascular calcification. Am J Kidney Dis. 2011;58(5):826-34.

54. Parzych KR, Klionsky DJ. An overview of autophagy: morphology, mechanism, and regulation. Antioxid Redox Signal. 2014;20(3):460-73.

55. Mizushima N, Komatsu M. Autophagy: renovation of cells and tissues. Cell. 2011;147(4):728-41.

56. Oku M, Sakai Y. Three Distinct Types of Microautophagy Based on Membrane Dynamics and Molecular Machineries. Bioessays. 2018;40(6):e1800008.

57. Sahu R, Kaushik S, Clement CC, Cannizzo ES, Scharf B, Follenzi A, et al. Microautophagy of cytosolic proteins by late endosomes. Dev Cell. 2011;20(1):131-9.

58. Cuervo AM, Wong E. Chaperone-mediated autophagy: roles in disease and aging. Cell Res. 2014;24(1):92-104.

59. Vural A, Kehrl JH. Autophagy in macrophages: impacting inflammation and bacterial infection. Scientifica (Cairo). 2014;2014:825463.

60. Melendez A, Levine B. Autophagy in C. elegans. WormBook. 2009:1-26.

61. Popelka H, Klionsky DJ. Post-translationally-modified structures in the autophagy machinery: an integrative perspective. FEBS J. 2015;282(18):3474-88.

62. Kabeya Y, Mizushima N, Ueno T, Yamamoto A, Kirisako T, Noda T, et al. LC3, a mammalian homologue of yeast Apg8p, is localized in autophagosome membranes after processing. EMBO J. 2000;19(21):5720-8.

63. Huang R, Liu W. Identifying an essential role of nuclear LC3 for autophagy. Autophagy. 2015;11(5):852-3.

64. Johansen T, Lamark T. Selective autophagy mediated by autophagic adapter proteins. Autophagy. 2011;7(3):279-96.

65. Nezis IP, Stenmark H. p62 at the interface of autophagy, oxidative stress signaling, and cancer. Antioxid Redox Signal. 2012;17(5):786-93.

66. Bitto A, Lerner CA, Nacarelli T, Crowe E, Torres C, Sell C. P62/SQSTM1 at the interface of aging, autophagy, and disease. Age (Dordr). 2014;36(3):9626.

67. Bjorkoy G, Lamark T, Pankiv S, Overvatn A, Brech A, Johansen T. Monitoring autophagic degradation of p62/SQSTM1. Methods Enzymol. 2009;452:181-97.

68. Eknoyan G, Lameire N, Barsoum R, Eckardt KU, Levin A, Levin N, et al. The burden of kidney disease: improving global outcomes. Kidney Int. 2004;66(4):1310-4.

69. Saran R, Robinson B, Abbott KC, Agodoa LYC, Bhave N, Bragg-Gresham J, et al. US Renal Data System 2017 Annual Data Report: Epidemiology of Kidney Disease in the United States. Am J Kidney Dis. 2018;71(3S1):A7.

70. Goodman WG, Goldin J, Kuizon BD, Yoon C, Gales B, Sider D, et al. Coronary-artery calcification in young adults with end-stage renal disease who are undergoing dialysis. N Engl J Med. 2000;342(20):1478-83.

71. London GM. Cardiovascular calcifications in uremic patients: clinical impact on cardiovascular function. J Am Soc Nephrol. 2003;14(9 Suppl 4):S305-9.

72. Vervloet M, Cozzolino M. Vascular calcification in chronic kidney disease: different bricks in the wall? Kidney Int. 2017;91(4):808-17.

73. Amann K. Media calcification and intima calcification are distinct entities in chronic kidney disease. Clin J Am Soc Nephrol. 2008;3(6):1599-605.

74. London GM, Guerin AP, Marchais SJ, Metivier F, Pannier B, Adda H. Arterial media calcification in end-stage renal disease: impact on all-cause and cardiovascular mortality. Nephrol Dial Transplant. 2003;18(9):1731-40.

75. Kidney Disease: Improving Global Outcomes CKDMBDWG. KDIGO clinical practice guideline for the diagnosis, evaluation, prevention, and treatment of Chronic Kidney Disease-Mineral and Bone Disorder (CKD-MBD). Kidney Int Suppl. 2009(113):S1-130.

76. Hutchison AJ, Whitehouse RW, Boulton HF, Adams JE, Mawer EB, Freemont TJ, et al. Correlation of bone histology with parathyroid hormone, vitamin D3, and radiology in end-stage renal disease. Kidney Int. 1993;44(5):1071-7.

77. Monier-Faugere MC, Malluche HH. Trends in renal osteodystrophy: a survey from 1983 to 1995 in a total of 2248 patients. Nephrol Dial Transplant. 1996;11 Suppl 3:111-20.

78. Salusky IB, Coburn JW, Brill J, Foley J, Slatopolsky E, Fine RN, et al. Bone disease in pediatric patients undergoing dialysis with CAPD or CCPD. Kidney Int. 1988;33(5):975-82.

79. Ferreira A, Frazao JM, Monier-Faugere MC, Gil C, Galvao J, Oliveira C, et al. Effects of sevelamer hydrochloride and calcium carbonate on renal osteodystrophy in hemodialysis patients. J Am Soc Nephrol. 2008;19(2):405-12.

80. Malluche HH, Monier-Faugere MC. Risk of adynamic bone disease in dialyzed patients. Kidney Int Suppl. 1992;38:S62-7.

81. Nickolas TL, Leonard MB, Shane E. Chronic kidney disease and bone fracture: a growing concern. Kidney Int. 2008;74(6):721-31.

82. Jamal SA, Ljunggren O, Stehman-Breen C, Cummings SR, McClung MR, Goemaere S, et al. Effects of denosumab on fracture and bone mineral density by level of kidney function. J Bone Miner Res. 2011;26(8):1829-35.

83. Kim SM, Long J, Montez-Rath M, Leonard M, Chertow GM. Hip Fracture in Patients With Non-Dialysis-Requiring Chronic Kidney Disease. J Bone Miner Res. 2016;31(10):1803-9.

84. Cejka D, Parada-Rodriguez D, Pichler S, Marculescu R, Kramer I, Kneissel M, et al. Only minor differences in renal osteodystrophy features between wild-type and sclerostin knockout mice with chronic kidney disease. Kidney Int. 2016;90(4):828-34.

85. Eaton GJ, Custer RP, Johnson FN, Stabenow KT. Dystrophic cardiac calcinosis in mice: genetic, hormonal, and dietary influences. Am J Pathol. 1978;90(1):173-86.

86. Gorgels TG, Hu X, Scheffer GL, van der Wal AC, Toonstra J, de Jong PT, et al. Disruption of Abcc6 in the mouse: novel insight in the pathogenesis of pseudoxanthoma elasticum. Hum Mol Genet. 2005;14(13):1763-73.

87. Jiang Q, Oldenburg R, Otsuru S, Grand-Pierre AE, Horwitz EM, Uitto J. Parabiotic heterogenetic pairing of Abcc6-/-/Rag1-/- mice and their wild-type counterparts halts ectopic mineralization in a murine model of pseudoxanthoma elasticum. Am J Pathol. 2010;176(4):1855-62.

88. Meng H, Vera I, Che N, Wang X, Wang SS, Ingram-Drake L, et al. Identification of Abcc6 as the major causal gene for dystrophic cardiac calcification in mice through integrative genomics. Proc Natl Acad Sci U S A. 2007;104(11):4530-5.

89. Berndt A, Li Q, Potter CS, Liang Y, Silva KA, Kennedy V, et al. A single-nucleotide polymorphism in the Abcc6 gene associates with connective tissue mineralization in mice similar to targeted models for pseudoxanthoma elasticum. J Invest Dermatol. 2013;133(3):833-6.

90. Le Saux O, Fulop K, Yamaguchi Y, Ilias A, Szabo Z, Brampton CN, et al. Expression and in vivo rescue of human ABCC6 disease-causing mutants in mouse liver. PLoS One. 2011;6(9):e24738.

91. El-Abbadi MM, Pai AS, Leaf EM, Yang HY, Bartley BA, Quan KK, et al. Phosphate feeding induces arterial medial calcification in uremic mice: role of serum phosphorus, fibroblast growth factor-23, and osteopontin. Kidney Int. 2009;75(12):1297-307.

92. Qiao JH, Fishbein MC, Demer LL, Lusis AJ. Genetic determination of cartilaginous metaplasia in mouse aorta. Arterioscler Thromb Vasc Biol. 1995;15(12):2265-72.

93. Rieg T. A High-throughput method for measurement of glomerular filtration rate in conscious mice. J Vis Exp. 2013(75):e50330.

94. Sedej S, Schmidt A, Denegri M, Walther S, Matovina M, Arnstein G, et al. Subclinical abnormalities in sarcoplasmic reticulum Ca(2+) release promote eccentric myocardial remodeling and pump failure death in response to pressure overload. J Am Coll Cardiol. 2014;63(15):1569-79.

95. Foley RN, Parfrey PS, Sarnak MJ. Epidemiology of cardiovascular disease in chronic renal disease. J Am Soc Nephrol. 1998;9(12 Suppl):S16-23.

96. Lanzer P, Boehm M, Sorribas V, Thiriet M, Janzen J, Zeller T, et al. Medial vascular calcification revisited: review and perspectives. Eur Heart J. 2014;35(23):1515-25.

97. Zoccali C, London G. Con: vascular calcification is a surrogate marker, but not the cause of ongoing vascular disease, and it is not a treatment target in chronic kidney disease. Nephrol Dial Transplant. 2015;30(3):352-7.

98. Bover J, Evenepoel P, Urena-Torres P, Vervloet MG, Brandenburg V, Mazzaferro S, et al. Pro: cardiovascular calcifications are clinically relevant. Nephrol Dial Transplant. 2015;30(3):345-51.

99. McIntyre CW. Calcium balance during hemodialysis. Semin Dial. 2008;21(1):38-42.

100. Block GA, Klassen PS, Lazarus JM, Ofsthun N, Lowrie EG, Chertow GM. Mineral metabolism, mortality, and morbidity in maintenance hemodialysis. J Am Soc Nephrol. 2004;15(8):2208-18.

101. Cannata-Andia JB, Martin KJ. The challenge of controlling phosphorus in chronic kidney disease. Nephrol Dial Transplant. 2016;31(4):541-7.

102. Paloian NJ, Giachelli CM. A current understanding of vascular calcification in CKD. Am J Physiol Renal Physiol. 2014;307(8):F891-900.

103. Schlieper G, Schurgers L, Brandenburg V, Reutelingsperger C, Floege J. Vascular calcification in chronic kidney disease: an update. Nephrol Dial Transplant. 2016;31(1):31-9.

104. Proudfoot D, Skepper JN, Hegyi L, Bennett MR, Shanahan CM, Weissberg PL. Apoptosis regulates human vascular calcification in vitro: evidence for initiation of vascular calcification by apoptotic bodies. Circ Res. 2000;87(11):1055-62.

105. Owens GK, Kumar MS, Wamhoff BR. Molecular regulation of vascular smooth muscle cell differentiation in development and disease. Physiol Rev. 2004;84(3):767-801.

106. Foley RN, Collins AJ, Herzog CA, Ishani A, Kalra PA. Serum phosphorus levels associate with coronary atherosclerosis in young adults. J Am Soc Nephrol. 2009;20(2):397-404.

107. Foley RN. Phosphate levels and cardiovascular disease in the general population. Clin J Am Soc Nephrol. 2009;4(6):1136-9.

108. Adeney KL, Siscovick DS, Ix JH, Seliger SL, Shlipak MG, Jenny NS, et al. Association of serum phosphate with vascular and valvular calcification in moderate CKD. J Am Soc Nephrol. 2009;20(2):381-7.

109. Shobeiri N, Adams MA, Holden RM. Vascular calcification in animal models of CKD: A review. Am J Nephrol. 2010;31(6):471-81.

110. Kirsch AH, Smaczny N, Riegelbauer V, Sedej S, Hofmeister A, Stojakovic T, et al. Regulatory T cells improve nephrocalcinosis but not dystrophic cardiac calcinosis in DBA/2 mice. Am J Pathol. 2013;183(2):382-90.

111. Kirsch AH, Kirsch A, Artinger K, Schabhuttl C, Goessler W, Klymiuk I, et al. Heterogeneous susceptibility for uraemic media calcification and concomitant inflammation within the arterial tree. Nephrol Dial Transplant. 2015;30(12):1995-2005.

112. Nussenzweig SC, Verma S, Finkel T. The role of autophagy in vascular biology. Circ Res. 2015;116(3):480-8.

113. Choi AM, Ryter SW, Levine B. Autophagy in human health and disease. N Engl J Med. 2013;368(19):1845-6.

114. Yin Z, Pascual C, Klionsky DJ. Autophagy: machinery and regulation. Microb Cell. 2016;3(12):588-96.

115. Feng Y, He D, Yao Z, Klionsky DJ. The machinery of macroautophagy. Cell Res. 2014;24(1):24-41.

116. Mizushima N, Yoshimori T, Levine B. Methods in mammalian autophagy research. Cell. 2010;140(3):313-26.

117. Komatsu M, Waguri S, Koike M, Sou YS, Ueno T, Hara T, et al. Homeostatic levels of p62 control cytoplasmic inclusion body formation in autophagy-deficient mice. Cell. 2007;131(6):1149-63.

118. Dai XY, Zhao MM, Cai Y, Guan QC, Zhao Y, Guan Y, et al. Phosphate-induced autophagy counteracts vascular calcification by reducing matrix vesicle release. Kidney Int. 2013;83(6):1042-51.

119. Peng YQ, Xiong D, Lin X, Cui RR, Xu F, Zhong JY, et al. Oestrogen Inhibits Arterial Calcification by Promoting Autophagy. Sci Rep. 2017;7(1):3549.

120. Frauscher B, Kirsch AH, Schabhüttl C, Schweighofer K, Kétszeri M, Pollheimer M, et al. Autophagy Protects From Uremic Vascular Media Calcification. 2018;9(1866).

121. Mackenzie NC, Zhu D, Longley L, Patterson CS, Kommareddy S, MacRae VE. MOVAS-1 cell line: a new in vitro model of vascular calcification. Int J Mol Med. 2011;27(5):663-8.

122. Zoccali C, Vanholder R, Massy ZA, Ortiz A, Sarafidis P, Dekker FW, et al. The systemic nature of CKD. Nat Rev Nephrol. 2017;13(6):344-58.

123. Bowling CB, Inker LA, Gutierrez OM, Allman RM, Warnock DG, McClellan W, et al. Age-specific associations of reduced estimated glomerular filtration rate with concurrent chronic kidney disease complications. Clin J Am Soc Nephrol. 2011;6(12):2822-8.

124. Gagnon RF, Gallimore B. Characterization of a mouse model of chronic uremia. Urol Res. 1988;16(2):119-26.

125. Eller P, Eller K, Kirsch AH, Patsch JJ, Wolf AM, Tagwerker A, et al. A murine model of phosphate nephropathy. Am J Pathol. 2011;178(5):1999-2006.

126. Nikolov IG, Joki N, Nguyen-Khoa T, Ivanovski O, Phan O, Lacour B, et al. Chronic kidney disease bone and mineral disorder (CKD-MBD) in apolipoprotein E-deficient mice with chronic renal failure. Bone. 2010;47(1):156-63.

127. Gonzalez EA, Lund RJ, Martin KJ, McCartney JE, Tondravi MM, Sampath TK, et al. Treatment of a murine model of high-turnover renal osteodystrophy by exogenous BMP-7. Kidney Int. 2002;61(4):1322-31.

128. Leroux-Berger M, Queguiner I, Maciel TT, Ho A, Relaix F, Kempf H. Pathologic calcification of adult vascular smooth muscle cells differs on their crest or mesodermal embryonic origin. J Bone Miner Res. 2011;26(7):1543-53.

129. Graciolli FG, Neves KR, Barreto F, Barreto DV, Dos Reis LM, Canziani ME, et al. The complexity of chronic kidney disease-mineral and bone disorder across stages of chronic kidney disease. Kidney Int. 2017;91(6):1436-46.

130. Battaglia M, Stabilini A, Roncarolo MG. Rapamycin selectively expands CD4+CD25+FoxP3+ regulatory T cells. Blood. 2005;105(12):4743-8.

131. Battaglia M, Stabilini A, Draghici E, Gregori S, Mocchetti C, Bonifacio E, et al. Rapamycin and interleukin-10 treatment induces T regulatory type 1 cells that mediate antigen-specific transplantation tolerance. Diabetes. 2006;55(1):40-9.

132. Yamada S, Tokumoto M, Tatsumoto N, Taniguchi M, Noguchi H, Nakano T, et al. Phosphate overload directly induces systemic inflammation and malnutrition as well as vascular calcification in uremia. Am J Physiol Renal Physiol. 2014;306(12):F1418-28.

133. Shoji-Kawata S, Sumpter R, Leveno M, Campbell GR, Zou Z, Kinch L, et al. Identification of a candidate therapeutic autophagy-inducing peptide. Nature. 2013;494(7436):201-6.

134. Sun Q, Fan J, Billiar TR, Scott MJ. Inflammasome and autophagy regulation - a two-way street. Mol Med. 2017;23.

135. Deretic V, Saitoh T, Akira S. Autophagy in infection, inflammation and immunity. Nat Rev Immunol. 2013;13(10):722-37.

136. Levine B, Mizushima N, Virgin HW. Autophagy in immunity and inflammation. Nature. 2011;469(7330):323-35.

137. Cadwell K. Crosstalk between autophagy and inflammatory signalling pathways: balancing defence and homeostasis. Nat Rev Immunol. 2016;16(11):661-75.

138. Saitoh T, Fujita N, Jang MH, Uematsu S, Yang BG, Satoh T, et al. Loss of the autophagy protein Atg16L1 enhances endotoxin-induced IL-1beta production. Nature. 2008;456(7219):264-8.

139. Das G, Shravage BV, Baehrecke EH. Regulation and function of autophagy during cell survival and cell death. Cold Spring Harb Perspect Biol. 2012;4(6).

140. Nakahara T, Sato H, Shimizu T, Tanaka T, Matsui H, Kawai-Kowase K, et al. Fibroblast growth factor-2 induces osteogenic differentiation through a Runx2 activation in vascular smooth muscle cells. Biochem Biophys Res Commun. 2010;394(2):243-8.

141. Montes de Oca A, Madueno JA, Martinez-Moreno JM, Guerrero F, Munoz-Castaneda J, Rodriguez-Ortiz ME, et al. High-phosphate-induced calcification is related to SM22alpha promoter methylation in vascular smooth muscle cells. J Bone Miner Res. 2010;25(9):1996-2005.

142. Satomi-Kobayashi S, Kinugasa M, Kobayashi R, Hatakeyama K, Kurogane Y, Ishida T, et al. Osteoblast-like differentiation of cultured human coronary artery smooth muscle cells by bone morphogenetic protein endothelial cell precursor-derived regulator (BMPER). J Biol Chem. 2012;287(36):30336-45.